Banacos, P. C., M. L. Ekster, J. W. Dellicarpini, and E. J. Lyons, 2012: A multiscale analysis of the 1 June 2011 Northeast U.S. severe weather outbreak and associated Springfield, Massachusetts tornado. *Electronic J. Severe Storms Meteor.*, **7** (7), 1-40.

Electronic Journal of
SEVERE STORMS METEOROLOGY

A Multiscale Analysis of the 1 June 2011 Northeast U.S. Severe Weather Outbreak and Associated Springfield, Massachusetts Tornado

PETER C. BANACOS
NOAA / National Weather Service, Burlington, Vermont

MICHAEL L. EKSTER
NOAA / National Weather Service, Gray, Maine

JOSEPH W. DELLICARPINI
NOAA / National Weather Service, Taunton, Massachusetts

ERIC J. LYONS
Engineering Department, University of Massachusetts, Amherst, Massachusetts

(Submitted 28 March 2012; in final form 20 September 2012)

ABSTRACT

On 1 June 2011, the 12th killer tornado in New England since 1950 tracked 63 km (39 mi) from Westfield to Charlton, MA resulting in 3 fatalities, 200 injuries, and EF3 damage. At least fourteen supercells produced six confirmed tornadoes and six hail reports ≥7 cm (≥2.75 in) in diameter across eastern New York and New England. This paper takes a multiscale look at meteorological factors contributing to this event. The synoptic pattern evolution closely resembles the composite mean shown by Banacos and Ekster (2010) for significant severe weather events in the northeast United States associated with an elevated mixed layer (EML). The presence of an EML and rich boundary-layer moisture (surface dewpoints 20–22°C) supported surface-based CAPE >4000 J kg^{-1} by early afternoon on 1 June. A strengthening prefrontal trough within the moist and unstable boundary layer, together with increasing low and deep-layer shear created an environment favorable for tornadic supercells. In particular, storms moved into an environment with increasing values of 0–1-km AGL bulk shear, increasing storm relative helicity, and lower lifted condensation level heights. Values of these parameters were largely consistent with significant-tornado occurrence in proximity studies. Tornadic signatures in WSR-88D and experimental CASA 3-cm dual-polarization radar data are described, in addition to a remarkable three-body scatter spike associated with lofted debris near peak apparent intensity of the EF3 tornado.

1. Introduction

On 1 June 2011, at least fourteen supercell thunderstorms moved across eastern New York and New England yielding nearly 200 reports of severe weather (Fig. 1) including six confirmed tornadoes and six reports of hail ≥7 cm (≥2.75 in) in diameter. The most notable tornado caused 3 fatalities, 200 injuries, and produced EF3 damage on the Enhanced Fujita Scale (McDonald et al. 2003). This up to 0.8 km (0.5 mi) wide tornado (Fig. 2) moved along a 63-km (39-mi) path from Westfield to Charlton in south-central Massachusetts, including through the city of Springfield (population ~153 000, 2010 census).

The climatological frequency of *significant* tornadoes (defined here as ≥EF2) is relatively low across eastern New York (east of ~74°W) and New England; only 150 (2.4 y^{-1}) have been documented from 1950–2011, on 108 event days (1.7 y^{-1} average, 1 y^{-1} median). A similarly sized area of Oklahoma and Kansas or Mississippi and Alabama averages 20–25 such

Corresponding author address: Peter Banacos, NOAA/NWS/Weather Forecast Office, 1200 Airport Dr., South Burlington, VT 05403.
E-mail: peter.banacos@noaa.gov.

tornadoes per year. Only 12 killer tornadoes have occurred in New England since 1950 (Fig. 3).

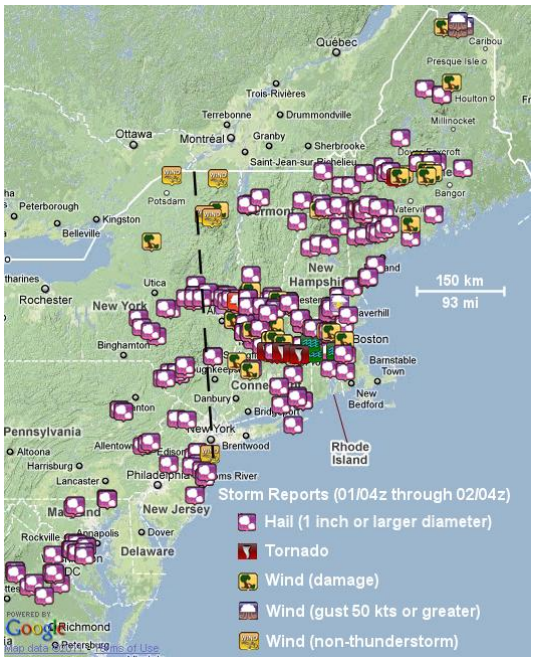

Figure 1: Preliminary local storm reports for the period 0400 UTC 1 June 2011 through 0400 UTC 2 June 2011. Black dashed line is western edge of climatological domain used in Table 1. *Click image to enlarge*.

To put the events of 1 June 2011 into further context, tornado days over eastern New York and New England (east of the black dashed line shown in Fig. 1) were quantified using the destruction potential index (DPI; Thompson and Vescio 1998) back to 1950. The DPI is:

$$DPI = \sum_{i=1}^{n} (pathlength_i \cdot pathwidth_i)(F_i + 1) \quad (1)$$

with n the number of tornadoes on a given day, and the path length, path width, and EF- / F-scale rating (F_i) used in aggregate for each tornado.

In terms of DPI, 1 June 2011 is the third-ranked tornado day, trailing only 10 July 1989 and 9 June 1953[1] (Table 1). The normalized, multivariate approach proposed by Doswell et al. (2006) also was applied to the same geographic area, using DPI, fatality and injury data. This normalized ranking placed 1 June 2011 at fourth behind 9 June 1953, 10 July 1989, and 3 October 1979. Since the multivariate statistics were normalized only for a region, it is not possible to compare these results to other U.S. outbreaks, as can be done more easily using DPI. Individual killer tornadoes ≥EF3 across the U.S. in 2011 also were ranked via DPI, with the Springfield tornado being 22nd of 37. The 10 significant hail reports (≥5.1 cm) and six baseball-sized or larger hail reports (≥7 cm) represent a single-day record for the region examined since 1950.

The paucity of tornadic supercells in the northeast U.S. is partly a result of factors that mitigate CAPE, namely stabilizing marine influences and the climatological infrequency of steep midtropospheric lapse rates (Farrell and Carlson 1989). However, these factors occasionally can be overcome in specific synoptic settings. Elevated mixed layers (EMLs; Carlson and Ludlum 1968; Lanicci and Warner 1991a,b,c) originating from the Intermountain West can be transported distances >3000 km in subsiding, anticyclonically curved flow regimes. The eventual entrainment of a residual EML, in synoptic ascent ahead of an eastward advancing shortwave trough from the Great Lakes region, allows for steep midtropospheric lapse rates. Related thermal profiles contribute to CAPE

Figure 2: Video capture of the long-tracked EF3 tornado as it moved through Monson, MA around 2100 UTC 1 June 2011. [Provided by Monson Fire Department.] *Click image to enlarge.*

[1] For perspective, the record DPI for the United States is 2647 associated with the 3–4 April 1974 "Super Outbreak".

Figure 3: Plot of all killer tornado start and end points across New England since 1950. Annotations show date of occurrence and EF-Scale / F-Scale rating. *Click image to enlarge.*

values above climatological average (Banacos and Ekster 2010). These steep lapse rates allow for greater instability for both upward and downward parcel displacements, and bolster overall convective updraft and downdraft strength. Also, EML-associated strong and violent tornado events in New England typically occur in westerly to northwesterly mid-level flow (Johns and Dorr 1996) with sufficient low-level directional shear from south to west-northwest. The absence of an easterly or southeasterly low-level flow is important for tornado potential, as it limits the areal extent of stable marine modified air over land from the cool North Atlantic.

This paper has two goals. The first is to supplement the Banacos and Ekster (2010) composite study using a recent EML severe weather case in the northeast U.S. with the full benefit of modern operational datasets on the synoptic, mesoscale, and storm scale. This affords the reader a diagnostic look at how an EML-associated severe weather event unfolds from beginning to end. Storm environment details not included in the composite study due to its broader scope and historical nature are discussed here. Second, several important radar observations are presented, including a "debris spike" in WSR-88D data and dual-polarization products from the Collaborative Adaptive Sensing of the Atmosphere (CASA) radar at UMASS-Amherst (McLaughlin et al. 2009).

A "forecast funnel" approach (Snellman 1982; Schultz 2010) is used to present this case study, starting with a synoptic-scale analysis in section 2, a mesoscale analysis in section 3, and a radar-based examination of the storm scale in section 4. Aspects of the resultant tornado damage are discussed in section 5. A concluding summary is presented in section 6.

Table 1: The top–20 tornado days over eastern New York and New England from 1950–2011 as ranked by Destruction Potential Index (DPI). Combined path length (CPL) is shown in km. The total number of tornado days over the area from 1950–2011 is 356, and the count of significant-tornado days is 108. Fatality (Fatal) and injury (Inj) information is from *Storm Data*.

Rank	DATE	# of TORs	DPI	CPL	Fatal	Inj	NOTABLE TORs
1	10 July 1989	13	**160.6**	100.3	0	141	Hampden, CT (F4)
2	9 Jun 1953	5	**132.1**	105.6	90	1228	Worcester, MA (F4)
3	*1 Jun 2011*	*6*	***81.0***	*87.9*	*3*	*200*	*Springfield, MA (EF3)*
4	24 July 2008	1	**75.7**	81.3	1	2	Epsom, NH (EF2)
5	31 May 1998	5	**70.4**	68.9	0	68	Mechanicville, NY (F3)
6	3 Oct 1979	1	**44.9**	18.2	3	500	Windsor Locks, CT (F4)
7	29 May 1995	3	**17.7**	45.9	3	29	Great Barrington, MA (F4)
8	21 Aug 2009	1	**13.1**	26.4	0	0	Norway, ME (EF1)
9	3 Jul 1997	10	**12.2**	55.5	0	1	Greenfield, NH (F2)
10	24 Jun 1960	1	**10.9**	17.5	0	9	Schenectady Co., NY (F3)
11	21 Aug 1951	4	**9.6**	93.7	0	17	Fairfield Co., CT (F3)
12	28 Aug 1973	3	**9.6**	19.6	4	11	W. Stockbridge, MA (F4)
13	18 Jun 1970	1	**9.4**	30.1	0	0	Central MA (F1)
14	7 Aug 1986	7	**8.4**	22.2	0	20	Providence, RI (F2)
15	8 Aug 1986	1	**8.0**	11.3	0	0	North Smithfield, RI (F1)
16	16 Jun 1974	1	**7.5**	79.0	0	0	Albany, NY (F3)
17	3 Oct 1970	4	**6.6**	82.7	1	1	Worcester Co., MA (F3)
18	21 Jul 2003	13	**6.0**	69.7	0	8	Columbia Co., NY (F2)
19	12 Jul 2006	1	**5.2**	16.3	0	6	Westchester Co., NY (F2)
20	13 Jun 1961	2	**4.2**	21.4	0	0	Franklin Co., VT (F2)

2. Synoptic setting

The synoptic setup on the afternoon of 1 June 2011 featured a shortwave trough translating eastward across the central Great Lakes region (Fig. 4a), with strengthening deep-layer wind fields overspreading eastern New York and New England. At the surface, a well-defined prefrontal trough extended from north-northeast to south-southwest across far eastern New York southward across eastern Pennsylvania (Fig. 4b). The thermal structure of the prefrontal trough resembles that in Fig. 7d–f of Schultz (2005), where a warm anomaly develops ahead of the cold front. The warm anomaly in this case arises from both insolation and adiabatic descent in the lee of the Adirondack Mountains and Allegheny Plateau, which led to a sharpening pressure trough through the afternoon hours. The upstream cold front was located across southeast Ontario, and was associated with greater surface to 700-hPa baroclinicity than was the prefrontal trough (Fig. 4a and b). Between the prefrontal trough and cold front was a sharp dewpoint gradient (Fig. 4b) on the order of 8° C/100 km. It was between the dewpoint discontinuity and the prefrontal trough that daytime storms would initially develop (analyzed further in Section 3).

The synoptic-scale midtropospheric flow pattern preceding 1 June 2011 was favorable for the advection and maintenance of an EML plume into eastern New York and New England, and closely resembles the composite mean evolution for EML-associated significant severe weather days (Fig. 5 in Banacos and Ekster 2010). The long downstream transport of the EML is plausible via the lapse rate tendency equation (Air Weather Service 1990), and favored in observational composite analyses by anti-cyclonically curved flow. In this pattern, mid-level subsidence maintains the EML plume through downward stretching (i.e., differential subsidence in the vertical near the top of the capping inversion layer). Additionally, large-scale subsidence inhibits the formation of widespread convective storms upstream, thereby precluding deleterious moist convective overturning of the EML plume.

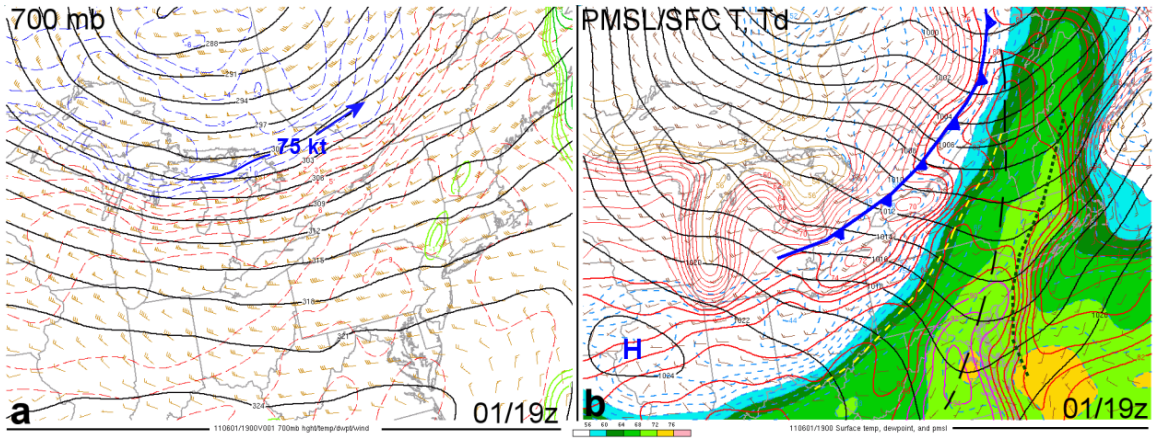

Figure 4: Storm Prediction Center RUC-based mesoanalysis showing a) 700-hPa geopotential height (black lines every 30 m), temperature (dashed lines every 1°C), wind barbs (kt), and jet axis (blue, with arrow); b) surface analysis showing sea-level pressure (black lines every 2 hPa), temperature (solid red lines every 2°F), and 2-m dewpoints (shaded, every 2°F) at 1900 UTC 1 June 2011. Surface prefrontal trough (black dashed line), dewpoint discontinuity (yellow dashed line), cold front, and moisture axis (dotted line) are denoted in panel (b). *Click image to enlarge.*

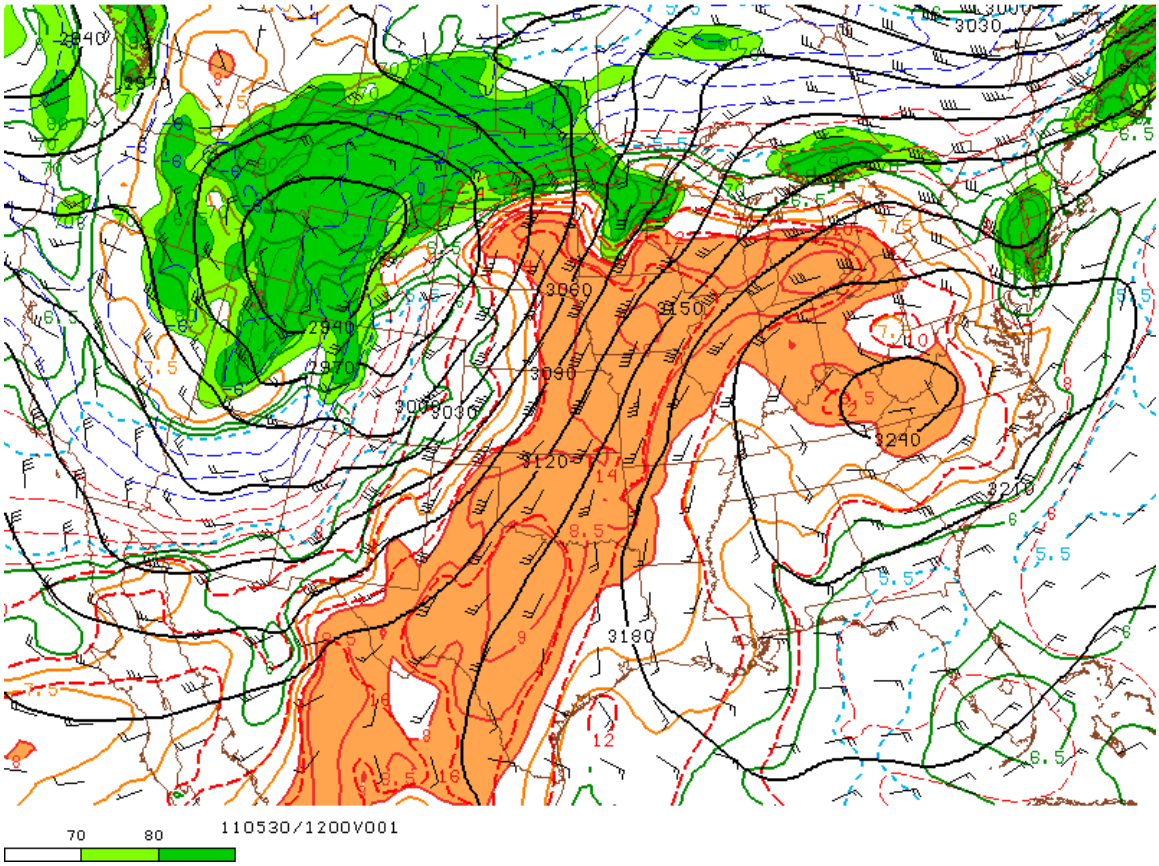

Figure 5: The 700-hPa analysis at 1200 UTC 30 May 2011 of geopotential height (black, solid lines at 30-m interval), relative humidity (%, shaded green above 70%), isotherms (every 2°C, dashed lines), wind barbs (pennant, full barb, and half-barb denote 25, 5, and 2.5 m s^{-1}, respectively), and 700–500-hPa lapse rates (solid red lines, with orange shading for values >8°C km^{-1}). *Click here for 6-hourly loop from 0000 UTC 28 May through 1800 UTC 01 June.*

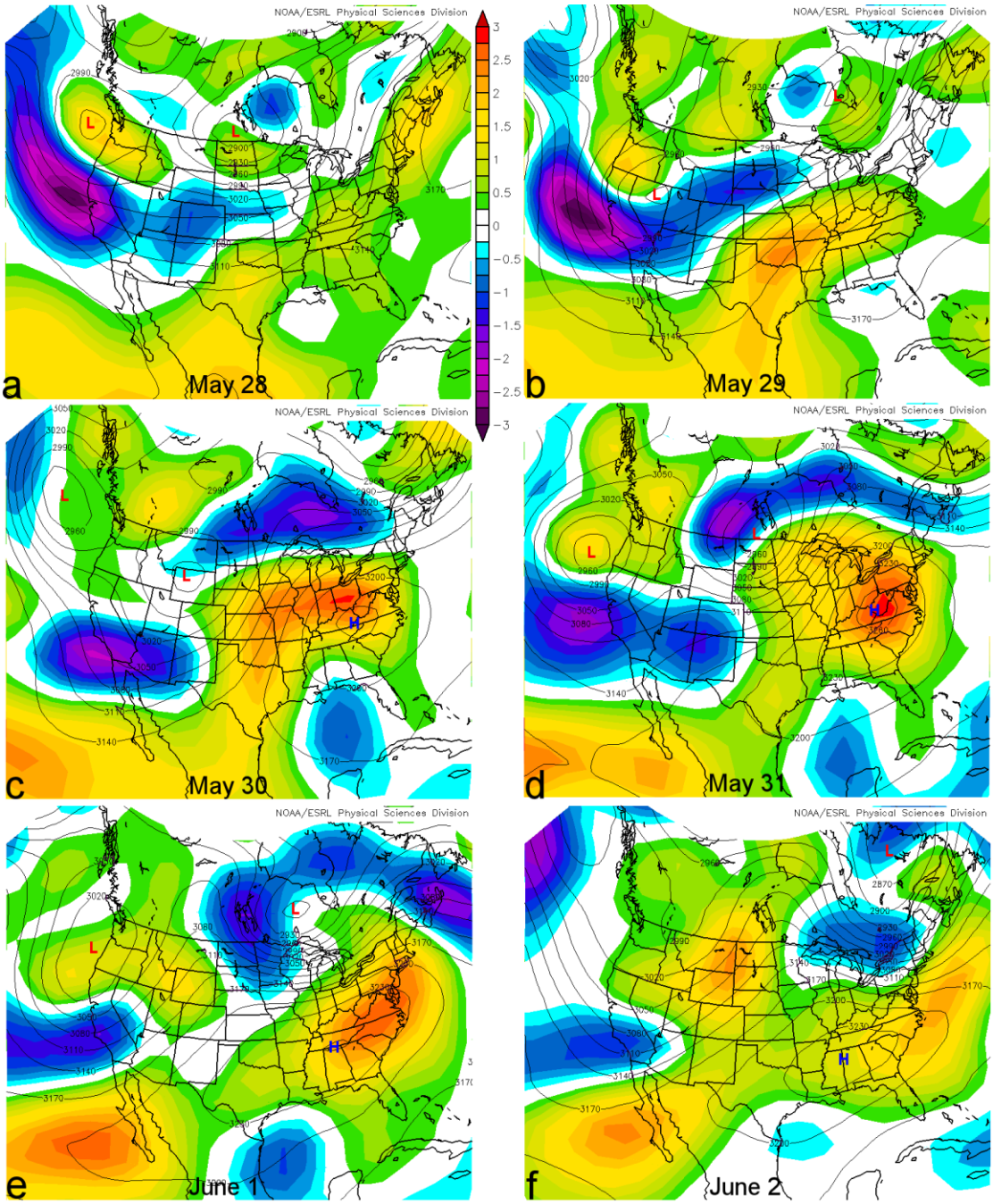

Figure 6: Mean daily 700-hPa geopotential heights (black lines, 30-m interval) and 700–500-hPa lapse rate anomalies vs. 1968–1996 climatology (shaded, 0.25°C km^{-1} interval) for a) 28 May, b) 29 May, c) 30 May, d) 31 May, e) 1 June, and f) 2 June. [From NCEP-NCAR Global Reanalysis.] *Click image to enlarge.*

The Rapid Update Cycle (RUC) based Storm Prediction Center (SPC) mesoanalysis (Bothwell et al. 2002) is useful in depicting the generation and subsequent movement of steep 700–500-hPa lapse rates associated with EMLs. The creation of very dry, deep mixed layers across the southern Rockies and Mexican plateau with daytime insolational heating is evident in the 6-hourly images displaying the 700-hPa analysis and 700–500-hPa lapse rates (Fig. 5). In the available image loop, a diurnal increase in areal coverage of 700–500-hPa lapse rates ≥8°C km^{-1} is apparent on 0000 UTC 28 May 2011 owing to deep mixing. The steep lapse-rate plume moved with the mean flow east-northeastward to become an EML across the lower elevations of

the Southern Plains into the mid-Mississippi River Valley on 28–29 May 2011. Within the strong anticyclonic curvature, the EML plume remained well-defined (i.e., it was not overturned by deep moist convection) and ultimately became entrained into the circulation of a building 700-hPa anticyclone across the eastern United States on 30–31 May. By 1 June, the 700-hPa ridge began to break down in response to a shortwave trough advancing eastward across the Great Lakes. Lapse rates in the 700–500-hPa layer remained 7–7.5°C km^{-1} across central New England at 1800 UTC 1 June 2011.

The movement of the EML plume also can be inferred by the daily mean 700–500-hPa lapse-rate anomalies (versus 1968–1996 climatology) based on National Centers for Environmental Prediction and National Center for Atmospheric Research (NCEP/NCAR) Reanalysis data (Kalnay et al. 1996) (Fig. 6a–f). The anomaly magnitude increased (≥3°C km^{-1}) as the plume reached the Ohio Valley and points east (Fig. 6c–d), a function of the relative rarity of such steep lapse rates over the eastern United States versus the Great Plains. On 1 June, 700–500-hPa lapse-rate anomalies on the order of 2–2.25°C km^{-1} are present over western Massachusetts (Fig. 6e), associated with mean absolute values of 7.5°to 8°C km^{-1}. The anomalies are shunted well south of New England with the arrival of the shortwave trough and more stable midtropospheric conditions on 2 June (Fig. 6f).

To confirm the origin and evolution of the EML plume, the NOAA Air Resources Laboratory Hybrid Single-Particle Lagrangian Integrated Trajectory (HYSPLIT) model (Draxler and Hess 1997, 1998) was used to create backward Lagrangian trajectories from the Albany, NY rawinsonde location (ALB) at 1200 UTC 1 June, from elevations of 3.5, 4, and 4.5 km AGL (Fig. 7a). The air can be traced back to Arizona and New Mexico at 0000 UTC 28 May, consistent with its inferred movement from the SPC mesoanalysis and global reanalysis data. The trajectories complete a full anticyclonic loop across the Ohio and Tennessee River valleys and central Appalachians; 10 of 36 EML-related significant-severe weather events similarly had mid-tropospheric trajectories that completed full anticyclonic loops in the composite EML study of Banacos and Ekster (2010). This emphasizes the importance of subsidence in maintaining the EML plume over long distances. Likewise, modest subsidence can be seen in the time-height cross section (Fig. 7a, bottom graph) during much of the traverse across the central and eastern U.S., especially from 0000 UTC 30 May through 0000 UTC 1 June.

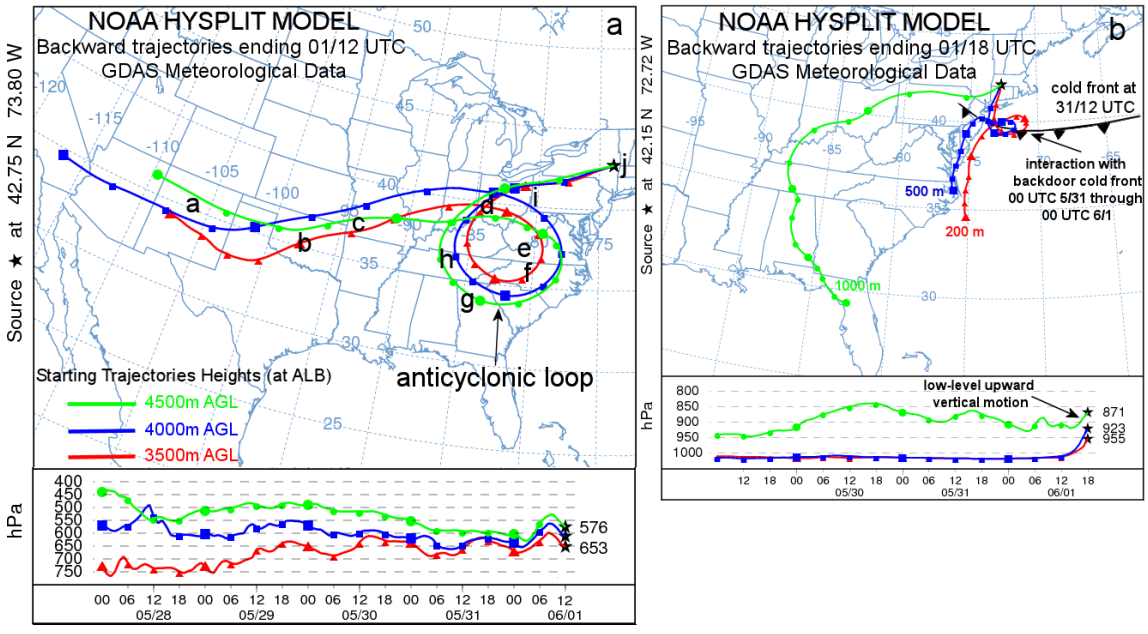

Figure 7: NOAA HYSPLIT model output for a) 108-h backward trajectories from Albany, NY (ALB) at 1200 UTC 1 June and b) 84-h backward trajectories from Westfield, MA (BAF). Letters denote rawinsonde locations shown in Fig. 8. Starting trajectory heights (at ALB) shown in legend. Bottom panel shows time-height cross section of each trajectory at 6-h intervals. *Click image to enlarge.*

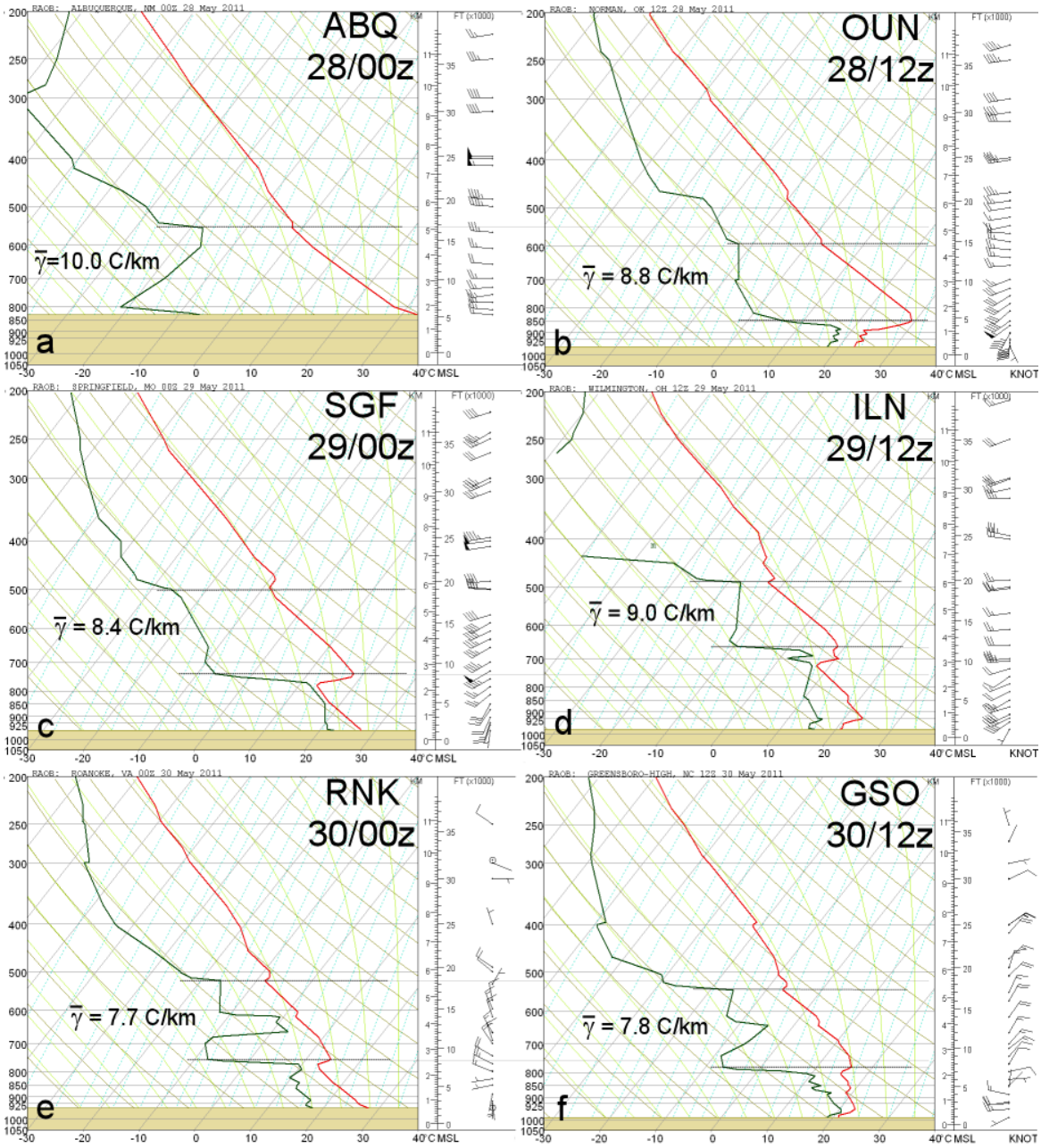

Figure 8: Skew*T*–log*p* diagrams of rawinsondes along backward trajectories in Fig. 6a, from a) Albuquerque, NM (ABQ), at 0000 UTC 28 May; b) Norman, OK (OUN), at 1200 UTC 28 May; c) Springfield, MO (SGF), 0000 UTC 29 May; d) Wilmington, OH (ILN) at 1200 UTC 29 May; e) Roanoke, VA (RNK) at 0000 UTC 30 May; f) Greensboro, NC (GSO) at 1200 UTC 30 May; g) Peachtree City, GA (FFC) at 0000 UTC 31 May; h) Nashville, TN (BNA) at 1200 UTC 31 May; i) Pittsburgh, PA (PIT) at 0000 UTC 1 June; and j) ALB at 1200 UTC 1 June. Horizontal dashed lines represent the EML boundary (the mixed-layer top at ABQ) based on the inflection points in the temperature profile, and mean lapse rates ($\bar{\gamma}$) are indicated in ^{o}C km^{-1} for that layer. *Click images to enlarge*

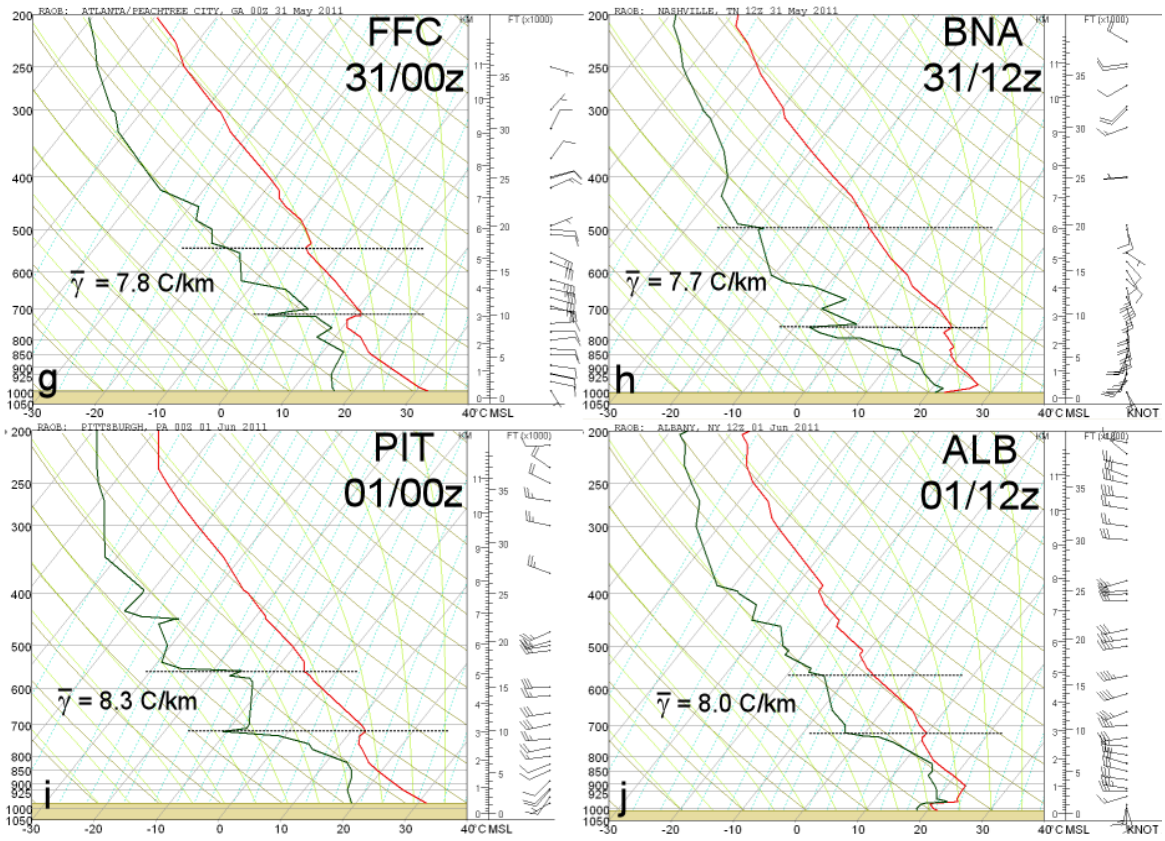

Figure 8 continued: *Click images to enlarge.*

Observed soundings along the HYSPLIT trajectories show the transition from a deep surface-based mixed layer at Albuquerque, NM (Fig. 8a) to an EML at Norman, OK (Fig. 8b) and Springfield, MO (Fig 8c). Steep lapse rates in the residual EML plume remain ≈8.0° C km^{-1} through a depth ≥150 hPa over a period of 4.5 days (108 h), ultimately reaching ALB at 1200 UTC 1 June (Fig. 8j). A 230-hPa deep layer at ALB has a mean lapse rate of 8.0°C km^{-1}, meeting the sounding criteria used by Banacos and Ekster (2010) in classifying EML-related significant severe weather events.

The low-level air (backward trajectories from 200 m, 500 m, 1000 m) in the vicinity of Springfield, MA was traced backward 84 h (Fig. 7b). Near-surface trajectories originating near the North Carolina coast moved north-northeastward, slowed during interaction with a cold front on 31 May (described in Section 3), and then accelerated north-northeastward reaching southwestern MA by 1800 UTC 1 June. The 1000-m backward trajectory took a more circuitous route with origins over Florida. These near-surface trajectories were associated with rich low-level moisture advection, and low-level ascent is apparent in all three in the hours leading up to 1800 UTC 1 June (Fig. 7b, bottom graph). The low- and mid-level trajectory analyses (Fig. 7a–b) show how the large-scale pattern collocated steep mid-level lapse rates with rich boundary-layer moisture (dewpoints 20–22° C), yielding the strongly unstable environment described in the following section.

3. Mesoscale analysis and convective parameters

a. Mesoscale conditions

Two episodes of convective storms occurred across eastern New York and New England on 1 June 2011, as is apparent in hourly mosaic composite reflectivity imagery (Fig. 9). The first storm clusters during the early morning hours were associated with midtropospheric differential vorticity advection (not shown) in an increasingly moist environment downstream of the shortwave trough translating eastward across the northern Great Lakes. The initial nocturnal convective storms were also

coincident with the leading edge of 700-hPa geopotential height falls (suggesting the onset of quasigeostrophic ascent) across northern New York and New England as the strong upper ridge began to weaken; geopotential heights decreased 50–60 m between 0600–1200 UTC. Several of these storms became severe, aided by the abnormally steep mid-level lapse rates with the EML plume (Fig. 8j). These storms produced damaging winds and large hail 3.2–4.4 cm (1.25–1.75 in) in diameter across central and northern New York and into northeastern Vermont between 0830 UTC and 1130 UTC (Fig. 1).

By 1400 UTC, most of the leading storms had reached the Gulf of Maine, with clear skies in the warm sector across most of New England westward into New York. Daytime convective initiation began between 1300–1500 UTC (Fig. 9). Surface-based convective inhibition (CINH) computed from the 1200 UTC 1 June soundings at Buffalo, NY (not shown) and ALB indicated values of –80 J kg^{-1} and –200 J kg^{-1}, respectively. Thus, it is not surprising that daytime convective initiation occurred largely between the terrain-induced pre-frontal trough and the upstream dewpoint discontinuity (Fig. 10), in the less-capped environment across central New York southwestward into north-central Pennsylvania.

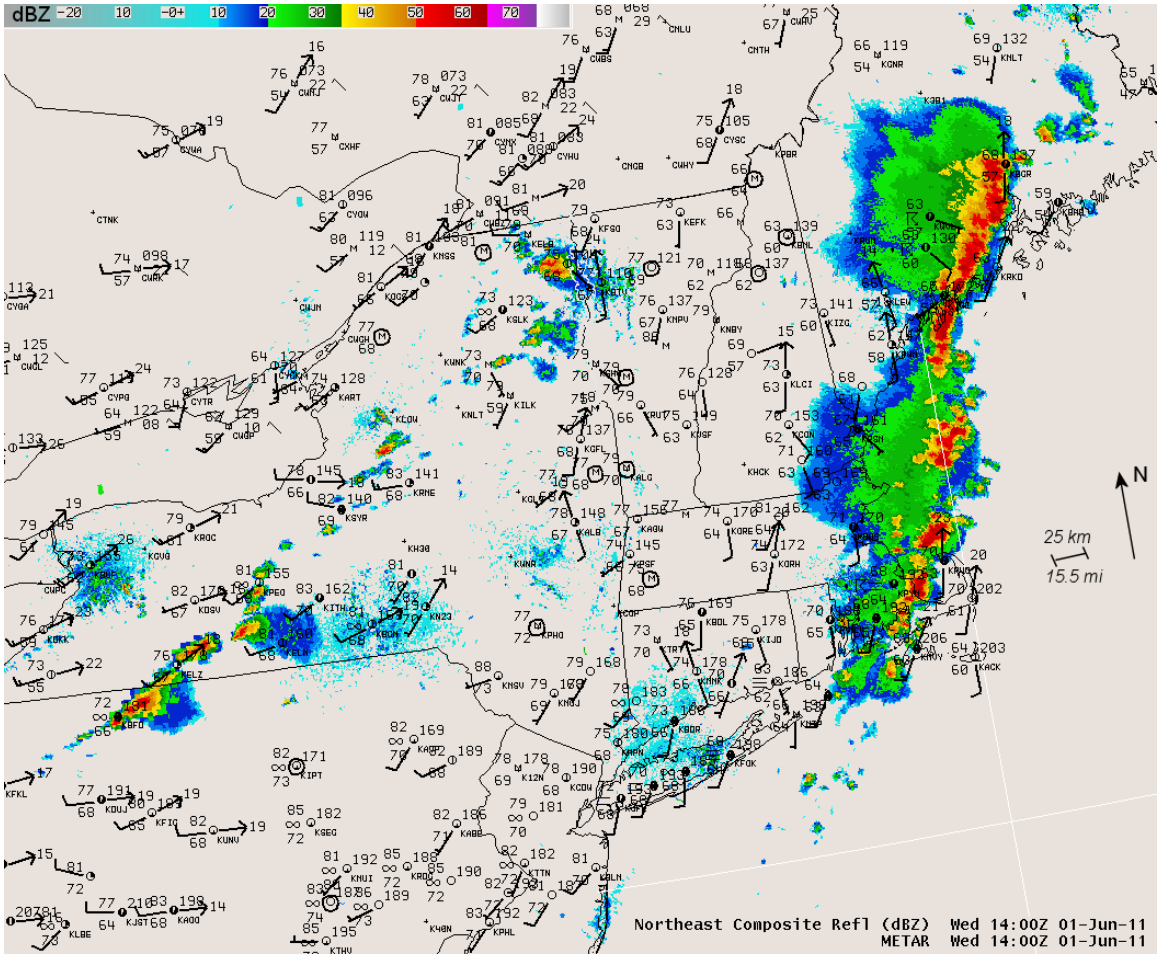

Figure 9: WSR-88D mosaic composite reflectivity (dB*Z*) and standard surface station model at 1400 UTC 1 June 2011, with temperature and dewpoint in °F. Pennant, full barb, and half-barb denote 25, 5, and 2.5 m s^{-1}, respectively. Arrows denote wind gusts in knots. *Click here for loop at 1-h interval from 0400 UTC through 2300 UTC. Click image to enlarge.*

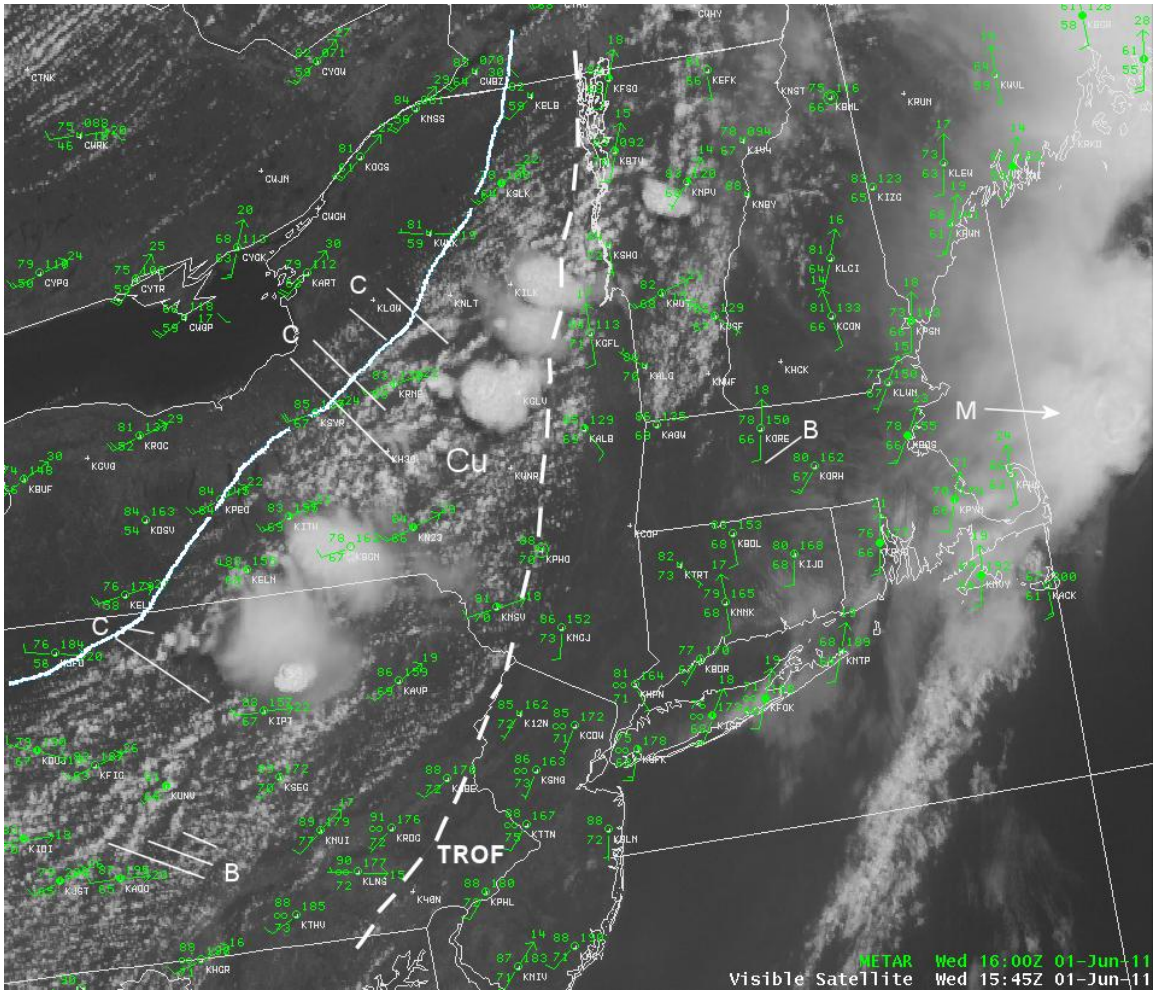

Figure 10: GOES-12 visible channel image at 1545 UTC 1 June 2011 and conventional surface observations (green) at 1600 UTC. Dashed line denotes position of prefrontal trough, and solid line denotes dewpoint break. Annotations denote the field of boundary-layer cumulus ("Cu"), transverse waves ("B"), initiating cloud bands ("C") and exiting early morning convective storms ("M"). *Click here for loop from 1315–2315 UTC. Click image to enlarge.*

West-central New York was also a region of increasing large-scale ascent provided by the approaching synoptic-scale trough from the west. The 0600 UTC 1 June North American Model (NAM; Janjić 2003) suggested low-level sloped isentropic ascent near the location of the initiating storms (Fig. 11). The cross section indicates that drying aloft and at the surface preceded the surface cold front (marked by the potential temperature gradient at 2100 UTC 1 June and 0000 UTC 2 June in the Fig. 11 loop) Daytime convective initiation occurred along a structure resembling a Pacific cold front without an associated surface temperature gradient (Locatelli et al. 2002). Any associated surface trough was ill-defined, masked by the more well-defined prefrontal trough over eastern New York and the upstream surface cold front. The boundary-layer air mass remained weakly capped at this time farther south and east, with transverse wave clouds evident over central Pennsylvania and more subtly over Connecticut Valley of west-central Massachusetts.

Storms became more numerous as they reached the Hudson Valley of New York, where the prefrontal trough and richer boundary-layer dewpoints in the low to mid 70s ºF were located. Based on visible satellite and composite radar imagery, more cells formed preferentially where longitudinal cloud bands in the deeply mixed air intersected the prefrontal trough (Fig. 10). These are inferred areas of enhanced convergence for updrafts. Periodic cell formation along the

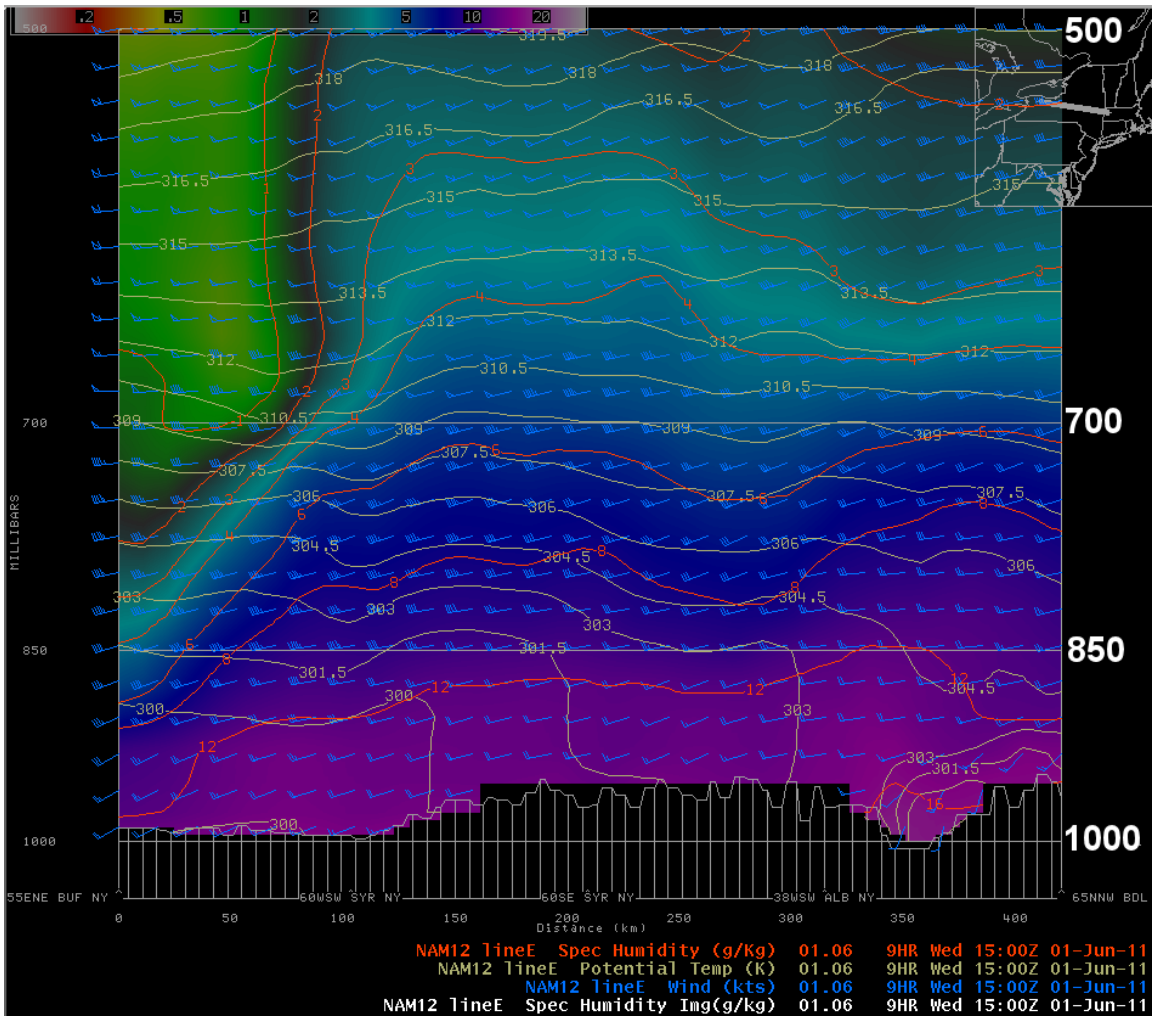

Figure 11: Vertical cross section from the 0600 UTC 1 June 2011 run of the North American Model (NAM) valid at 1500 UTC 1 June (9-h forecast) extending from western New York to western Massachusetts (see insert, top right). Fields include the potential temperature (beige, solid lines), specific humidity (red, solid lines and color fill), and wind (pennant, full barb, and half-barb denote 25, 5, and 2.5 m s^{-1}, respectively). Note strong drying above 850 hPa moving in from the west. *Click here for loop from 1500 UTC 1 June to 0000 UTC 2 June.*

prefrontal trough continued through 2300 UTC, perhaps also aided by upslope flow into the Berkshires of Massachusetts. These later rounds of storms would also produce severe weather and 3 additional tornadoes.

Many recent tornadic storms in New England have been documented along and downwind of prefrontal troughs (Cannon 2002). This empirical finding may be related to generally greater directional shear and richer moisture found downwind of the prefrontal trough consistent with the 1 June 2011 case. Time series analyses from Windsor Locks, CT (BDL) and ALB indicate that flow remained southerly with higher dewpoints throughout the afternoon east of the prefrontal trough, while the combination of veering winds west of the prefrontal trough and the movement of the dewpoint discontinuity into eastern New York yielded drier, more westerly surface winds at ALB (Fig. 12).

The favored long-lived supercellular convective mode observed on 1 June 2011 (detailed in Section 4) is also an important factor in tornado potential. In Fig. 4, there is a large normal component of the 700-hPa winds across

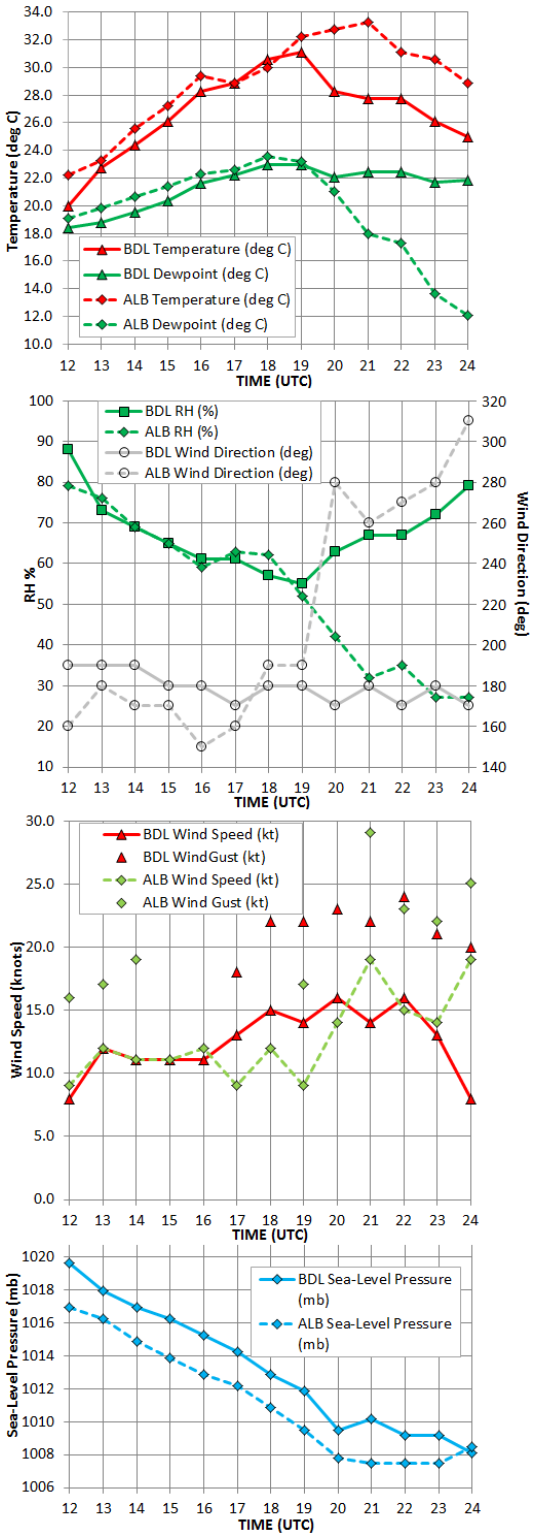

Figure 12: Time series of hourly weather as labeled, at Windsor Locks, CT (BDL; solid lines) and Albany, NY (KALB; dashed lines) from 1200 UTC 1 June through 0000 UTC 2 June.

the prefrontal trough, whereas the 700-hPa winds are stronger and somewhat more parallel near the surface cold front (as follows from the thermal wind relationship). Observational (Dial et al. 2010) and numerical studies (Bluestein and Weisman 2000) have demonstrated that the ability of convective storms to remain discrete for long periods in environments supporting supercells depends largely on the degree of cross-boundary flow of the cloud-layer wind. Storms readily move off the boundary limiting prolonged periods of linear ascent (and potential for squall-line development). We speculate that cloud-layer wind vectors are typically more orthogonal across most prefrontal troughs as compared to cold fronts in the region, supporting the importance of prefrontal troughs in observed tornado events in the northeast U.S.

Increasing deep-layer wind fields continued to overspread eastern New York and New England as the upper-level ridge weakened and the 700-hPa shortwave trough translated across the eastern Great Lakes region. The 700-hPa winds had increased to around 23 m s^{-1} (45 kt) near the prefrontal trough by 1900 UTC (Fig. 4a). Strong boundary-layer heating led to further strengthening of the prefrontal trough at 1900 UTC, coincident with a boundary-layer thermal axis approaching 32°C (90°F) (Fig. 4b, Fig. 12). Surface pressure falls of 1–1.5 hPa h^{-1} helped to strengthen near-surface wind fields, leading to increasing low-level directional and speed shear (Fig. 13) near the primary moisture axis from southeastern New York across southwestern Massachusetts into central New Hampshire and western Maine. Rich boundary-layer moisture was present (2-m dewpoints of 20–22°C) along the moisture axis (Fig. 4b), and remained steady or slowly increased across the area even as the daytime boundary layer deepened (Fig. 12). In general, dewpoints had increased during the prior 6–12 h as strengthening southerly to southwesterly low-level winds resulted in moisture return following the southward passage of a weak cold front on 31 May (Fig. 7b). While no well-defined mesoscale boundaries were present other than the prefrontal trough, the increased low-level moisture aided the convective environment. Near the tornado location, the surface conditions at Westfield, MA (BAF) were 32°C/22°C (90°F/72°F) at 1900 UTC; more-stable marine modified air was confined to coastal Massachusetts and Maine.

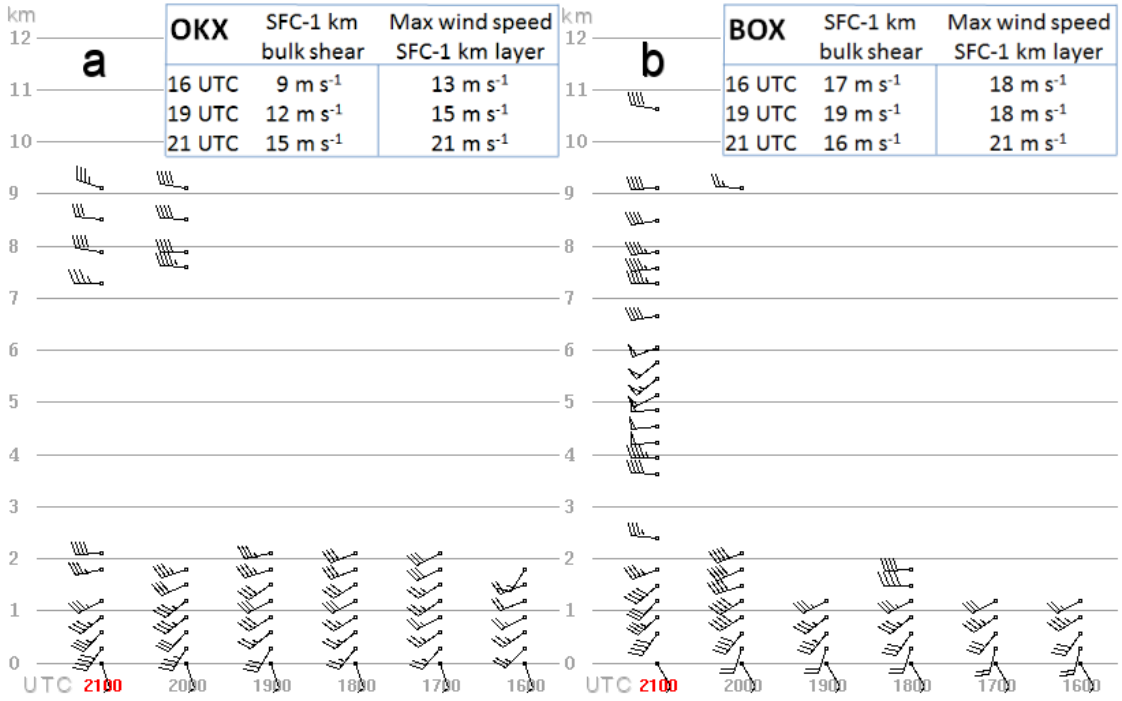

Figure 13: Hourly velocity-azimuth display wind profiles for a) Brookhaven, NY (OKX) and b) Taunton, MA (BOX) between 1600–2100 UTC 1 June 2011. Wind barbs represent 5 m s^{-1} (10 kt) and half barbs represent 2.5 m s^{-1} (5 kt). *Click image to enlarge.*

b. Convective parameters

In this section, we present commonly employed diagnostic variables as a means of assessing the convective environment on 1 June 2011 in the context of proximity studies. Convective parameters and indices represent *simplified* assessments of the true three-dimensional structure of the atmosphere, and the usual caveats concerning their operational use apply (e.g., Doswell and Schultz 2006).

As the ongoing convective storms moved eastward at 17 m s^{-1} (33 kt) into the moist axis, the SPC mesoanalysis fields at 1900 UTC indicated increasingly favorable conditions for tornadoes (Table 2). Most-unstable (MU) parcel CAPE reached 3500–4500 J kg^{-1} (Fig. 14a) and was coincident with westerly 0–6-km shear of 18–23 m s^{-1} (35–45 kt), values supporting supercells. Normalized CAPE (NCAPE, Blanchard 1998)— which takes the magnitude of CAPE divided by the depth of the CAPE layer— was unusually high at 0.3–0.4 m s^{-2} (not shown), a result of strong heating, rich boundary-layer moisture, and steep mid-level lapse rates associated with the EML. These values of NCAPE suggested strongly buoyant accelerations. Resultant updrafts and the observed supercellular storm mode supported hail greater than baseball size (>7 cm), as was observed in Windsor, MA and Shaftsbury, VT.

Wind vector magnitude difference (i.e., bulk shear) and storm relative helicity (SRH) in the surface to 1-km layer have been shown to discriminate well between significant-tornado (EF2 or greater) producing environments and supercell environments producing weak or no tornadoes in both parameter studies (Craven and Brooks 2004; Thompson et al. 2003; Rasmussen 2003) and field studies (e.g., Markowski et al. 1998). By 2000 UTC, 0–1-km AGL (hereafter, all elevations are AGL unless otherwise specified) bulk shear increased sharply to 12.5–15 m s^{-1} (25–30 kt; Fig. 15), consistent with radar-derived velocity-azimuth display wind trends (Fig. 13). The increase in low-level shear was likely a result of the surface pressure falls and strengthening gradient between the weakening 700-hPa ridge and approaching trough from the Great Lakes. The 0–1-km bulk shear was in the 75th–90th percentile range of the significant tornado parameter space shown in the RUC-based proximity study of Thompson et al.

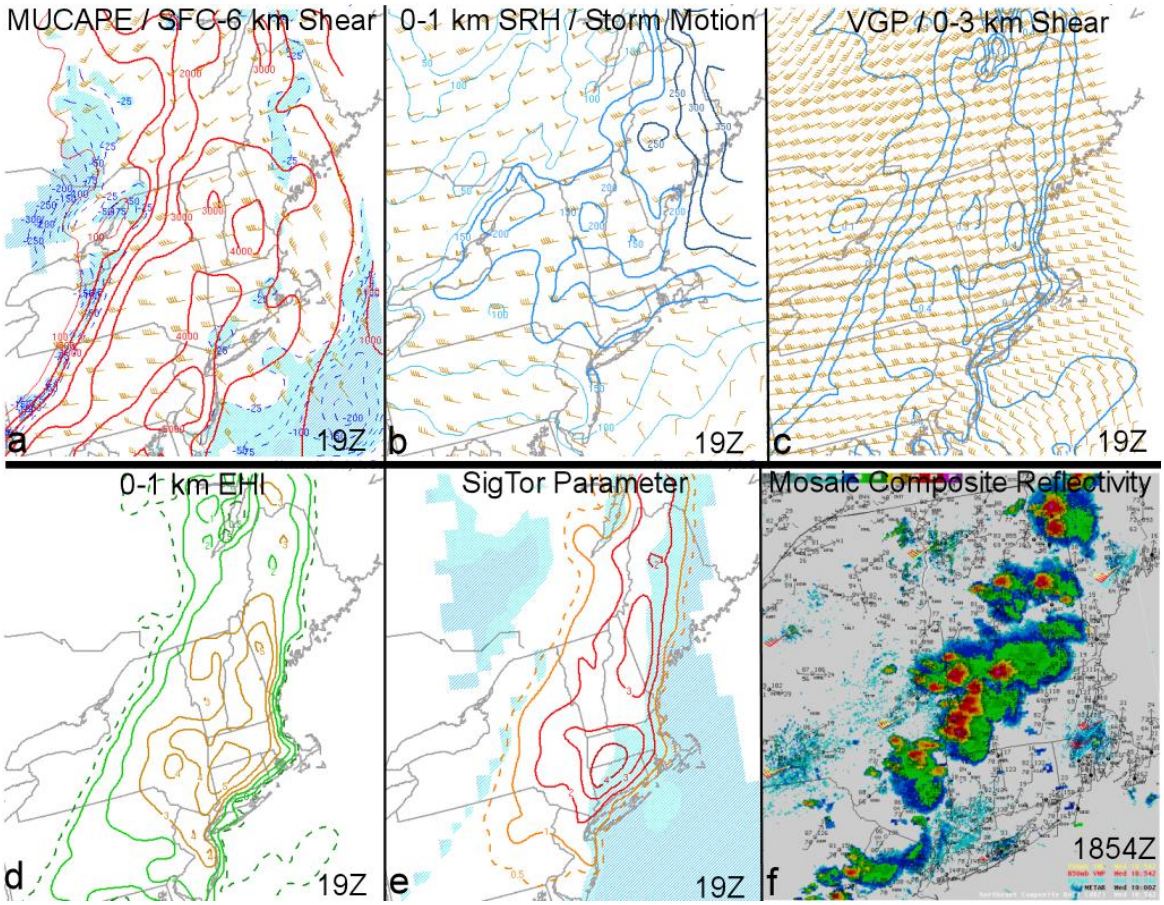

Figure 14: SPC mesoanalysis at 1900 UTC 1 June 2011 showing a) most-unstable CAPE (red lines, every 1000 J kg^{-1}) and 0–6-km bulk wind difference (kt); b) 0–1-km storm-relative helicity (m^{2}s^{-2}) and estimated storm motion (kt); c) vorticity generation parameter (m s^{-2}) and 0–3-km bulk wind difference (kt); d) the 0–1-km energy helicity index (EHI, non-dimensional); e) the significant tornado parameter (non-dimensional) and CIN <–25 J kg^{-1} (shaded); and f) the mosaic composite reflectivity and surface observations at 1854 UTC 1 June 2011. *Click here for composite reflectivity mosaic loop at 6-min interval. Click image to enlarge.*

(2003)[2]. The 0–1-km SRH was 200–250 m^2 s^{-2} (Fig. 14b), also within the significant tornado parameter space (Rasmussen 2003; Thompson et al. 2003). Increasing SRH east of the prefrontal trough was also evident in the BDL time series representative of the storm's inflow (Fig. 16). The vorticity generation parameter (VGP; Rasmussen and Blanchard 1998), combining low-level shear and CAPE, can be useful since it does not rely on an assumed storm motion. The 0–3 km VGP values >0.4 m s^{-2} (Fig. 14c) suggested strong rotational potential through vertical tilting of vorticity (Rasmussen and Blanchard 1998). The 0–3-km mixed layer CAPE (not shown) was near 150 J kg^{-1}, also in the significant-tornado class and important because of its theorized role in low-level stretching (Rasmussen 2003). The 0–1-km energy-helicity index (EHI) (Davies 1993) (Fig. 14d) and significant tornado parameter (STP) (Thompson et al. 2003) (Fig. 14e) values at 1900 UTC were also in the significant tornado parameter space (Rasmussen 2003, Thompson et al. 2003). Lastly, storms (Fig. 14f) were moving into an environment with progressively lower 100-hPa mean parcel lifted condensation level (MLLCL) heights, generally ≤1000 m from the Connecticut River valley eastward (Fig. 16); MLLCL heights of 1000 m are near the median of Thompson et al. (2003) for the significant-

[2] Given that the SPC mesoanalysis is based on 1-h RUC forecast grids (combined with observed surface conditions), a comparison of convective parameters to the parameter space in Thompson et al. (2003) has particular relevance.

tornado class. With the prevalent supercellular convective mode, as summarized by the rotational tracks product from the NSSL Warning Decision Support System-II (Smith and Elmore 2004) (Fig. 17), the near-surface shear and thermodynamic environment supported significant-tornado potential.

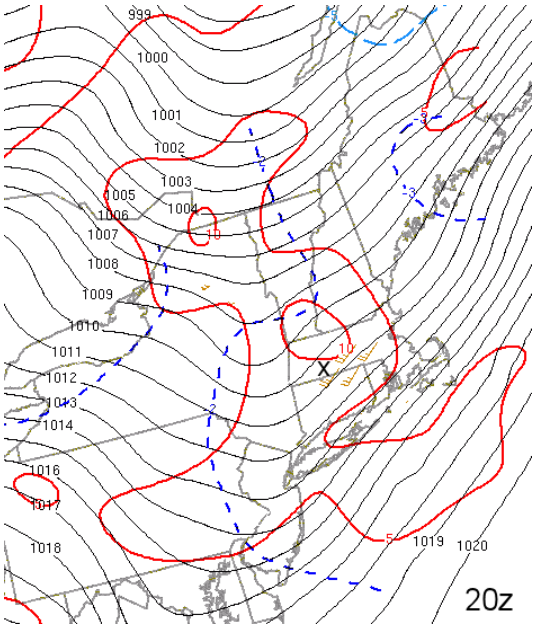

Figure 15: Sea-level pressure (hPa, black solid lines), 2-h isallobars (hPa, blue dashed lines), and 3-h change in 0–1-km bulk shear (m s^{-1}, red solid lines) at 2000 UTC 1 June 2011. Representative 0–1-km shear barbs (20–25 kt) shown near EF3 tornado location ("X") in south-central Massachusetts. *Click image to enlarge.*

c. Modified proximity sounding

A proximity sounding and hodograph were constructed using the observed rawinsonde from ALB at 1600 UTC 1 June. The ALB sounding was modified for 1900 UTC 1 June surface temperature, dewpoint, and wind conditions at BAF (temperature and dewpoint respectively at 32°C and 22°C, 90°F and 72°F) and an Aircraft Communications Addressing and Reporting System (ACARS) ascent sounding from BDL, for the winds below 500 hPa (Fig. 18). The low-level wind magnitude and hodograph curvature are consistent with mean proximity hodographs in significantly tornadic environments (e.g., see Markowski et al. 2003, their Fig. 12). Convective parameters are generally consistent with the SPC mesoanalysis values and are summarized in Table 2.

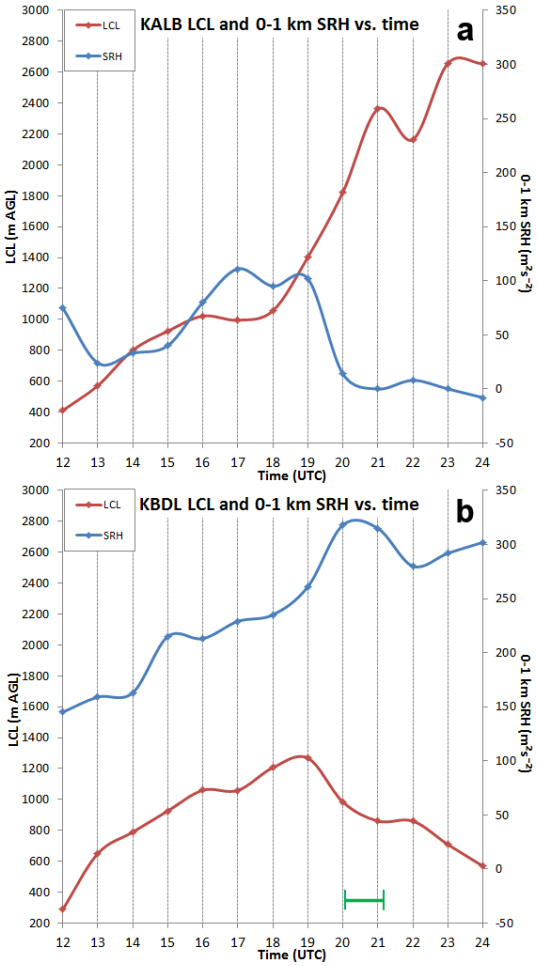

Figure 16: Time series of LCL height (m) and 0–1 km SRH (m^2s^{-2}) for a) ALB and b) BDL from 1200 UTC 1 June through 0000 UTC 2 June. Values derived from hourly METARs and ACARS and rawinsonde data (the latter for ALB only). Storm motions used were 267°/17 m s^{-1} at ALB and 270°/17 m s^{-1} at BDL. EF3 tornado lifespan labeled in green on panel (b). *Click image to enlarge.*

4. Storm-scale/radar analysis

a. WSR-88D analysis

By 1900 UTC 1 June 2011, intense thunderstorms were aligned from the Berkshire Mountains in Massachusetts northeastward to northwestern Maine (Fig. 14f). The storms were moving into an environment characterized by a combination of strong vertical shear and high CAPE that was relatively rare for New England (Fig. 14a). This regime supported classic supercells sampled by the WSR-88D network in

Table 2: Convective parameters at 1900 UTC 1 June 2011 near the starting location of the EF3 Springfield, MA tornado. Columns include RUC-based SPC mesoanalysis (values approximated over KBAF) and a modified 1600 UTC ALB sounding using KBAF surface conditions at 1900 UTC and an ACARS ascent sounding from BDL (24 km to the south) for winds below 500 hPa.

Parameter	SPC Mesoanalysis	Modified Sounding
SBCAPE	≈4000 J kg^{-1}	4452 J kg^{-1}
MLCAPE	3000–3500 J kg^{-1}	2422 J kg^{-1}
CAPE (0–3 km)	150 J kg^{-1}	163 J kg^{-1}
NCAPE	0.30–0.40 m s^{-2}	0.37 m s^{-2}
700–500 hPa Lapse Rate	7.5ºC km^{-1}	7.0ºC km^{-1}
MLLCL	1000 m	1146 m
Storm Motion (Bunkers)	270°/15 m s^{-1}	279°/14 ms^{-1}
Bulk Shear (0–1 km)	13 m s^{-1}	15 m s^{-1}
Bulk Shear (0–6 km)	23 m s^{-1}	24 m s^{-1}
SRH (0–1 km)	200–250 m^2 s^{-2}	261 m^2 s^{-2}
EHI (0–1 km)	5–6	8
VGP (0–3 km)	0.4–0.5 ms^{-2}	0.67 ms^{-2}

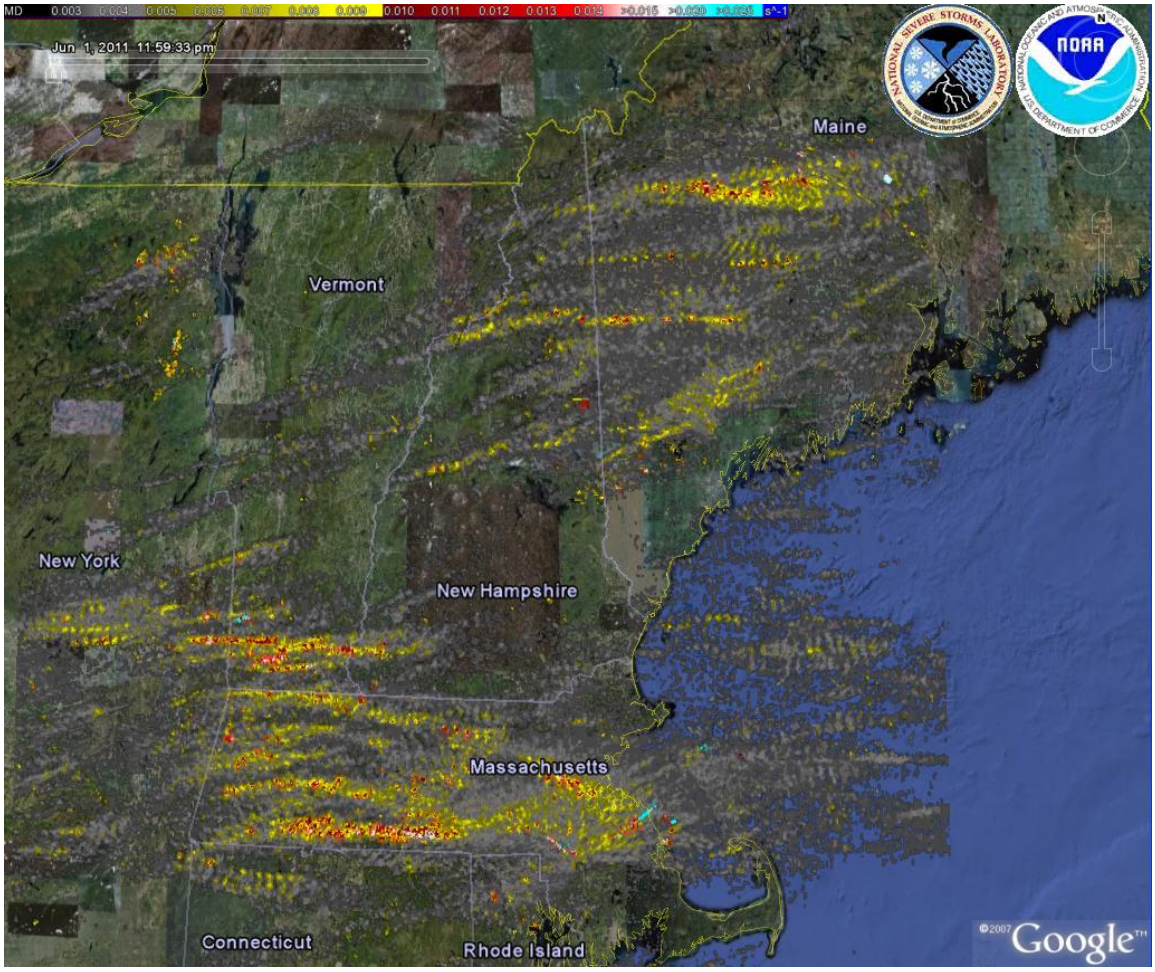

Figure 17: NSSL WDSS-II rotation tracks product for 1 June 2011. *Click image to enlarge.*

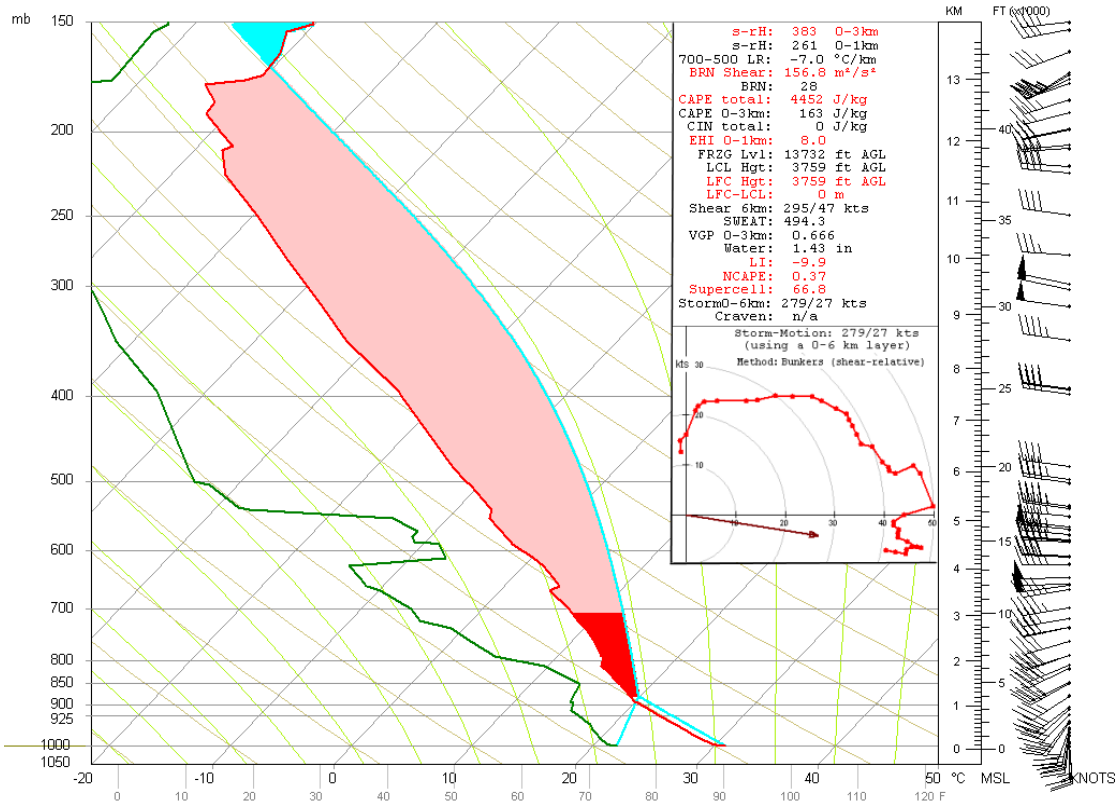

Figure 18: Skew*T*–log*p* diagram of the 1600 UTC 1 June 2011 Albany, NY (ALB) sounding modified for 1853 UTC surface temperature and dewpoint at Westfield, MA (BAF). Hodograph and wind profile below 500 hPa are based on surface winds at Westfield and the 2022 UTC ACARS sounding ascent from BDL. Parcel buoyancy is shaded; dark red shading represents 0–3 km AGL CAPE. *Click image to enlarge.*

New England and eastern New York. Impressive radar reflectivity and velocity signatures normally associated with strong and violent tornadoes in the central United States were observed in New England—particularly in association with the supercell that produced the EF3 tornado in Massachusetts (Fig. 19), which will be the focus of the following discussion.

A cluster of thunderstorms consisting mainly of supercells was moving eastward across western Massachusetts at 2015 UTC (Fig. 20a). The most noteworthy supercell was near Westfield, MA, receiving unimpeded, moist, southerly inflow due to its southernmost location with respect to the rest of the storm cluster. This cell produced the strong (EF3), long-tracked tornado that began in Westfield, MA at 2017 UTC and dissipated 63 km (39 mi) to the east in Charlton, MA. The 0.5° beam-elevation storm-relative motion product from the WSR-88D in East Berne, NY (KENX; the WSR-88D closest to the cell at the time) 2 min prior to tornadogenesis indicated a gate-to-gate shear couplet (25 m s^{-1} inbound, 31 m s^{-1} outbound velocities) near Westfield (Fig. 20b). The 0.5° base reflectivity at the same time did not reveal a hook echo (Fujita 1973) at the location of the velocity couplet, but rather a bounded weak echo region (BWER) (Lemon and Doswell 1979) surrounded by a ring of 15 to 25 dBZ echoes (Fig. 20a). A better-defined hook echo would not develop until approximately 15 min later, or about the time the tornado was moving through Springfield, MA.

As the tornadic supercell moved east of the Connecticut River Valley, the tornado widened and became more damaging (see Section 5) for elusive reasons. The leading cluster of storms located north and east of the tornadic supercell (Fig. 20) may have established an east–west oriented outflow boundary, further enhancing low-level SRH along the tornadic supercell track (Markowski et al. 1998). Distance from surrounding radars and the absence of surface data along the strongest portion of the tornado track leaves inconclusive evidence of an outflow boundary.

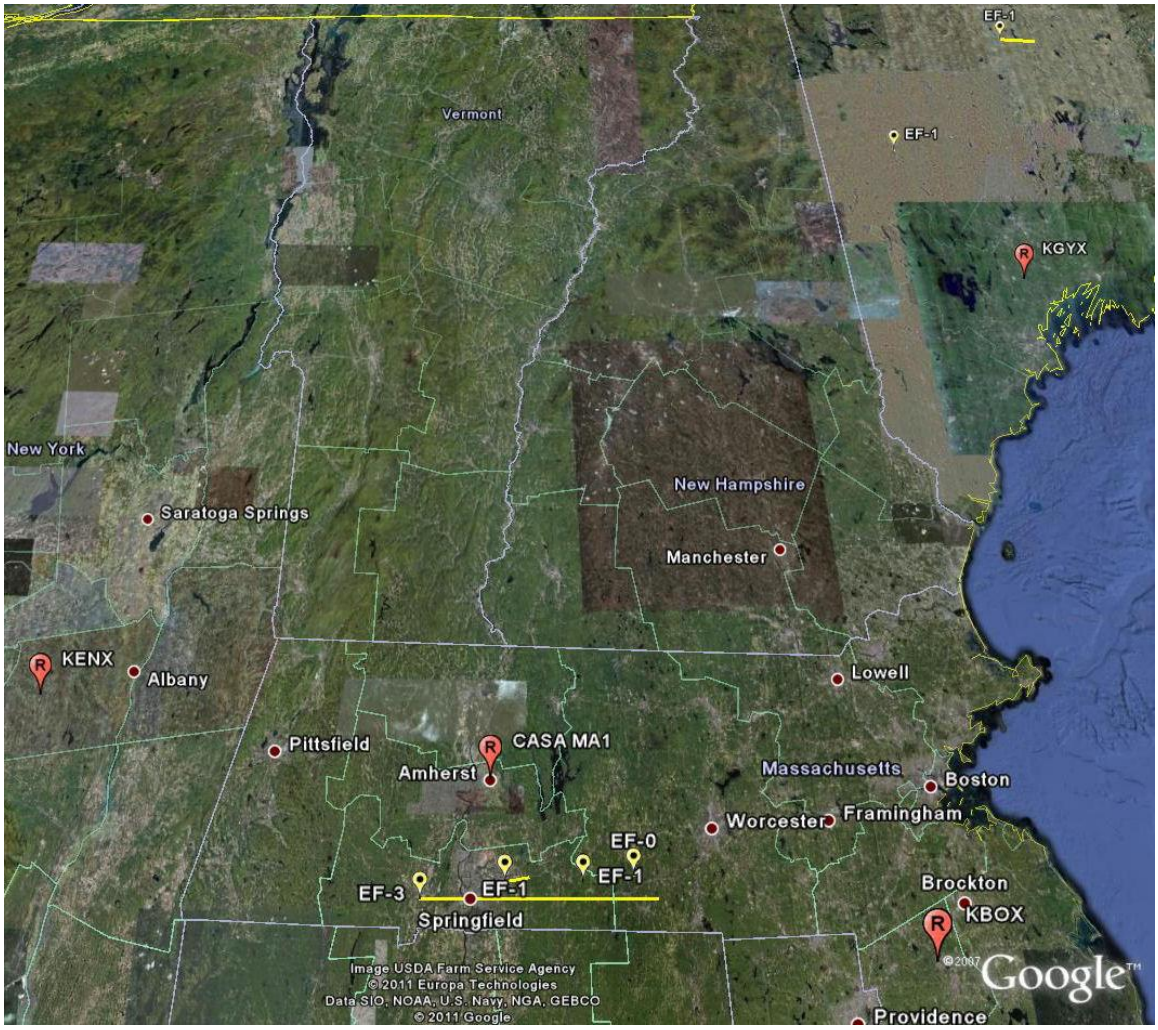

Figure 19: Tornado tracks (yellow lines) and EF-scale ratings in Massachusetts and Maine on 1 June 2011. Markers "R" refer to WSR-88D locations at East Berne, NY (KENX), Gray, ME (KGYX), and Taunton, MA (KBOX), and X-band radar at Amherst, MA (CASA MA1). *Click image to enlarge.*

In any event, during the 45-min period between approximately 2045–2130 UTC, the supercell took on radar-reflectivity characteristics similar to historic supercells that produced large, strong to violent tornadoes, such as those that occurred in Tuscaloosa, AL on 27 April 2011 and Moore, OK on 3 May 1999 (Fig. 21). These characteristics included a well-developed hook echo on the west or southwest flank of the parent supercell with an attendant "debris ball" (Bunkers and Baxter 2011). The debris ball is a circular area of enhanced reflectivity—often >60 dBZ—likely caused by beam backscattering off lofted debris (Fig. 22a). Though some cautionary exceptions have been noted (Bunkers and Baxter 2011), the presence of a debris ball usually indicates a tornado, especially when accompanied by a strong velocity shear couplet. Such a couplet was observed in this event with the strongest gate-to-gate shear at 2104 UTC (Fig. 22b). With the advent of dual-polarization radar, an unambiguous tornadic debris signature (TDS; Ryzhkov et al. 2005) includes the above reflectivity and velocity signatures in addition to collocated low correlation coefficient values, as shown in the CASA subsection[3].

Perhaps the most remarkable signature at the time of peak tornado rating was the presence of a three-body scatter signature (TBSS) emanating

[3] At the time of the event, the surrounding WSR-88D sites had not yet received their dual-polarization upgrades.

down-radial from the TDS itself (Fig. 22a). The presence of a TBSS in reflectivity and velocity fields historically has been documented as being a strong indicator of large hail (i.e., a "hail spike") due to Mie scattering of radar microwaves when the beam intersects large, wet hail (Zrnic 1987; Wilson and Reum 1986, 1988; Lemon 1998). In this case, it is presumed that Mie scattering off lofted large and/or wet debris in a heavily forested area was the primary cause of this TBSS or "debris spike" (J. Ladue, NOAA/NWS/WDTB personal communication). The debris spike was observed on 0.5° beam-elevation reflectivity imagery for five consecutive volume scans (2050–2109 UTC) as was a concurrent hail spike for four of those scans (2050–2104 UTC) (Fig. 23). The authors are unaware of any prior documentation of a TBSS emanating from a TDS.

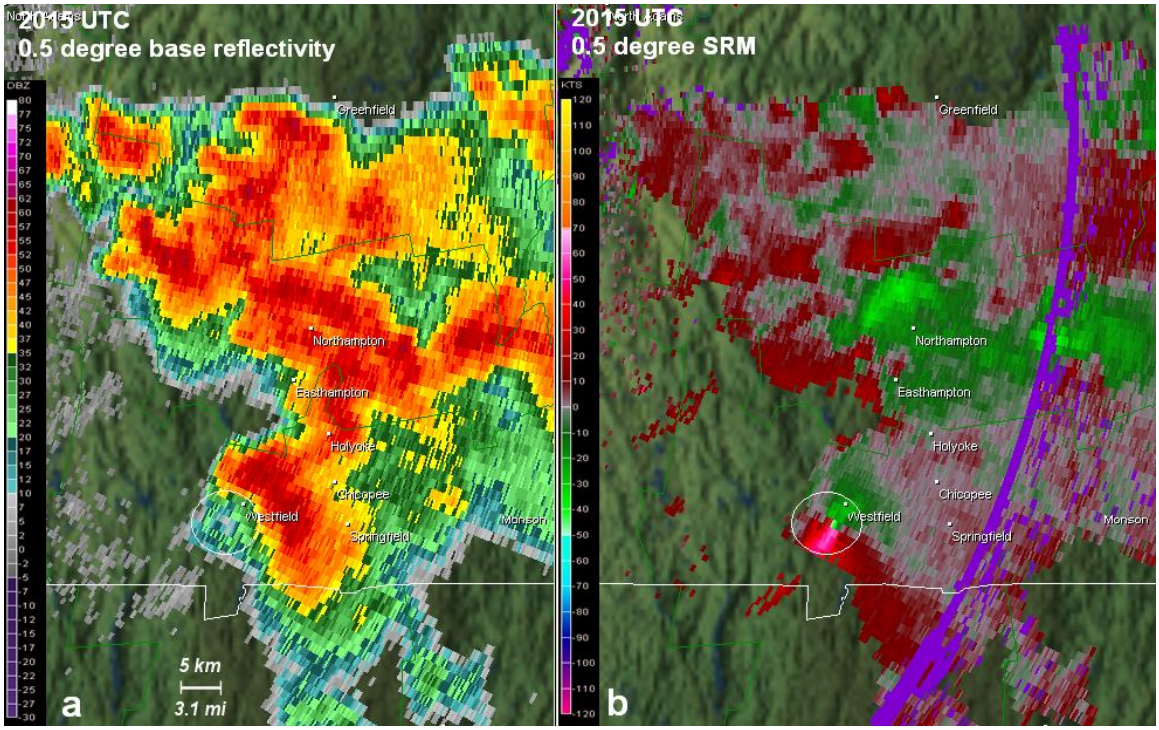

Figure 20: KENX 0.5° a) base reflectivity and b) storm relative velocity at 2015 UTC 1 June 2011. Circle denotes location of strong low-level mesocyclone near the time of tornadogenesis in Westfield, MA. *Click image to enlarge.*

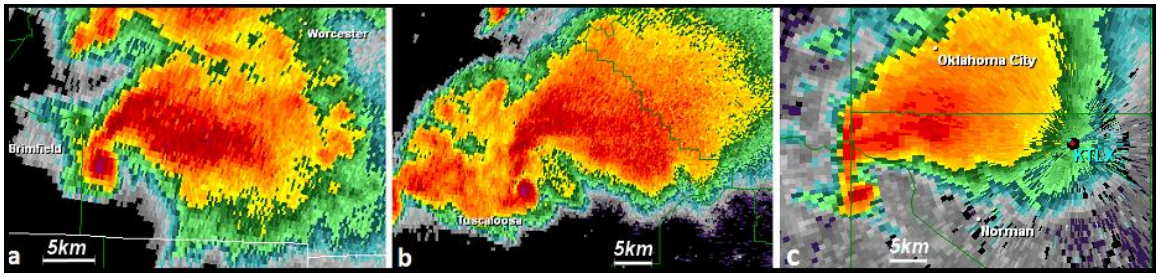

Figure 21: The 0.5° base reflectivity for a) Taunton, MA at 2113 UTC 1 June 2011, b) Birmingham, AL at 2219 UTC 27 April 2011 (Tuscaloosa, AL EF4), and c) Oklahoma City, OK (4-bit data) at 0002 UTC 4 May 1999 (Bridge Creek, OK F5). *Click image to enlarge.*

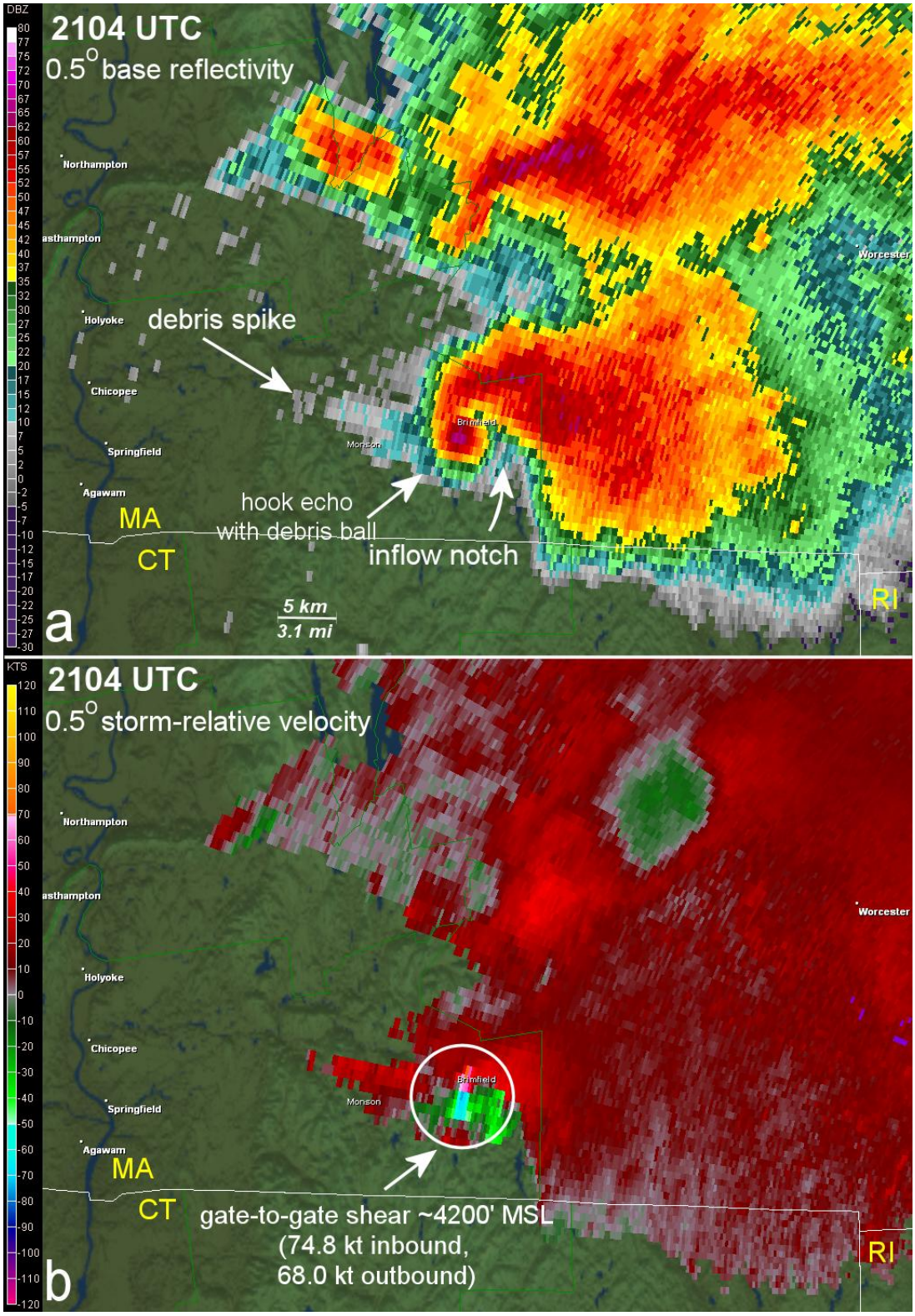

Figure 22: BOX 0.5° a) base reflectivity and b) storm relative velocity at 2104 UTC 1 June 2011, around time of tornado peak intensity near Brimfield, MA. Circle denotes location of strong mesocyclone. *Click here for loop of 0.5° base reflectivity and storm-relative velocity from 2013–2146 UTC. Click image to enlarge.*

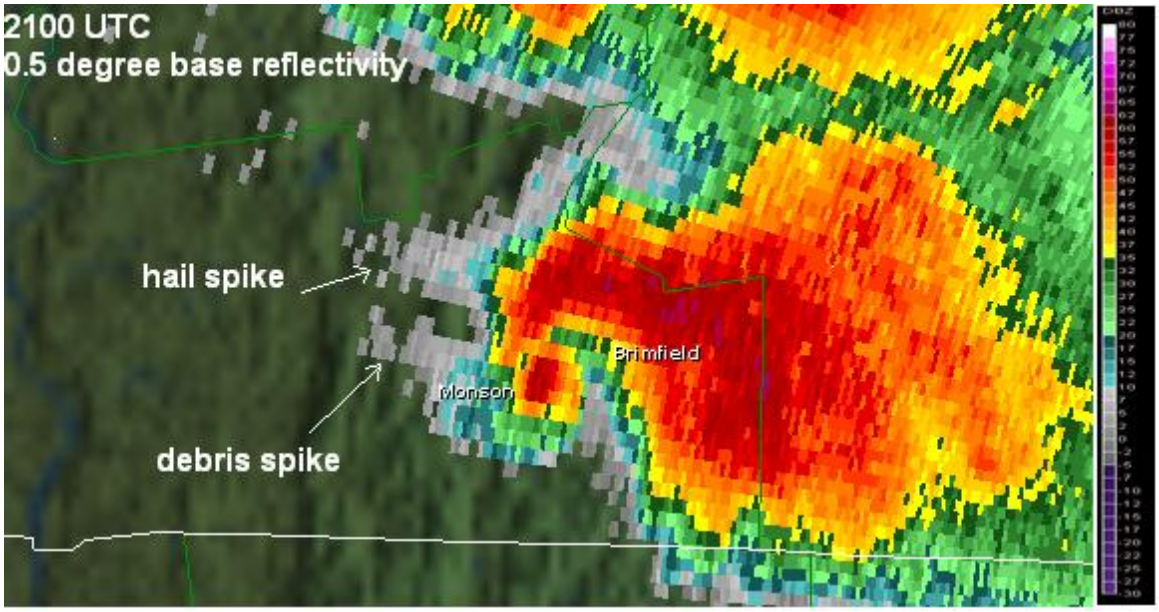

Figure 23: BOX 0.5° base reflectivity at 2100 UTC 1 June 2011 showing concurrent hail and debris spikes. *Click image to enlarge.*

Along-radial reflectivity and velocity cross sections were examined at 2104 UTC (Fig. 24a–b). These cross sections show several classic supercell features including a well-defined BWER and a deep, intense mesocyclone. Also present were the TDS and attendant debris spike. The debris spike was accompanied by near-zero or weak inbound radial velocities, consistent with classic TBSS signatures as described by Lemon (1998). A semi-transparent, three-dimensional reflectivity volume display also was generated (Fig. 25). Several noteworthy features can be visualized, including the mesocyclone, vault (or strong updraft region), and the debris plume which extended upward to ≈10 kft (3 km) above radar level (ARL). Some of the vertical tilt evident in the mesocyclone can be attributed to storm motion over the course of the volume scan, and there was no attempt to correct for this.

b. CASA radar analysis

The X-band (3-cm wavelength) CASA radar at Amherst, MA (CASA MA1; Fig. 19) also was collecting data for this case, performing 20-s surveillance sweeps at a fixed elevation of 3°. While attenuation in the presence of heavy precipitation is a drawback of X-band as compared to the 10-cm wavelength WSR-88D, these adaptive sensing dual-polarization radars have been shown to complement the WSR-88D network by providing higher spatial and temporal resolution with improved sampling of the lowest levels of the atmosphere (Schenkman et al. 2011; Wang and Chandrasekar 2010). A preliminary assessment of data collected by CASA MA1 follows.

The supercell that produced the long-tracked tornado across south-central Massachusetts was observed by the CASA MA1 as it progressed across Wilbraham into Monson and Brimfield. Prior to that, the tornado was not visible because of attenuation related to heavy precipitation near the radar. The attenuation eased as the tornadic storm neared the edge of the MA1 range [beam height of ≈6 kft (1.8 km) ARL] near the town of Monson at 2058 UTC (Fig. 26).

In the reflectivity hook echo (Fig. 26a), there was an "eye" at the center of the TDS likely due to outward centrifuging of debris and/or precipitation from the tornado (Dowell et al. 2005, Lewellen et al. 2008). The narrow filament of reflectivity associated with the remainder of the hook echo was associated mainly with high correlation coefficient values (ρ_{hv}) >0.95 and modest differential reflectivity (Z_{DR}) values of 3–4 dB (Fig. 26b), suggesting medium to large raindrops. Isolated higher Z_{DR} values (>5 dB) suggested very large drops or small melting hail. Dealiased velocities indicated 77 m s^{-1} (150 kt) of gate-to-gate shear in this region (Fig. 26c), or about 3.5 m s^{-1} (7 kt)

stronger than the maximum observed by BOX at2104 UTC (Fig. 22b). Consistent with other studies (e.g., Palmer et al. 2011; Bluestein et al. 2007; Ryzhkov et al. 2005), low correlation coefficient values around 0.8 (Fig. 26d) are found within the TDS, and are associated with the wide variety of non-hydrometeor reflectors lofted by the tornado itself. In the available loops (Fig. 26 caption), reflectivity, Z_{DR}, and ρ_{hv} elements "pulse" and travel along the axis of the hook echo, showing spatial and temporal drop-size discontinuities. The distribution of precipitation within supercell hook echoes is the subject of recent research with dual-polarization radar (e.g., Kumjian 2011).

5. Damage survey

The long-tracked tornado (Fig. 19) began in the Munger Hill section of Westfield, MA around 2017 UTC. The main form of damage in this area was uprooted or snapped trees. The roof of the Munger Hill Elementary School sustained minor damage. As the tornado tracked east through Westfield, it continued to uproot or snap large trees in the elevated Ridgeview Park area and Robinson State Park. Minor roof damage was observed to several homes. Tornado damage was rated EF1 with estimated wind speeds of 38–49 m s^{-1} (86–110 mph).

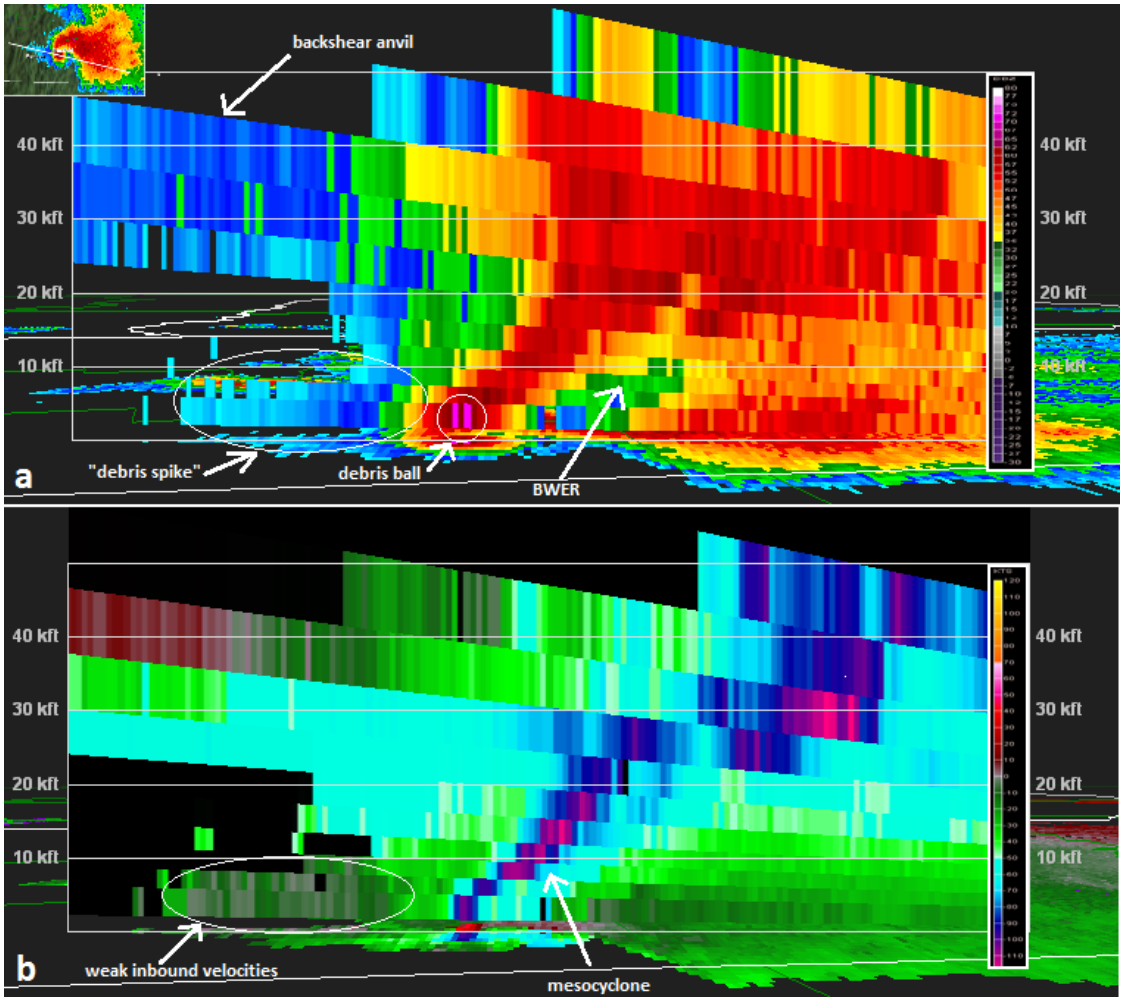

Figure 24: BOX vertical cross sections of a) reflectivity, and b) base velocity at 2104 UTC. Length of cross section baseline (inset, top left) is approximately 37 km. *Click image to enlarge.*

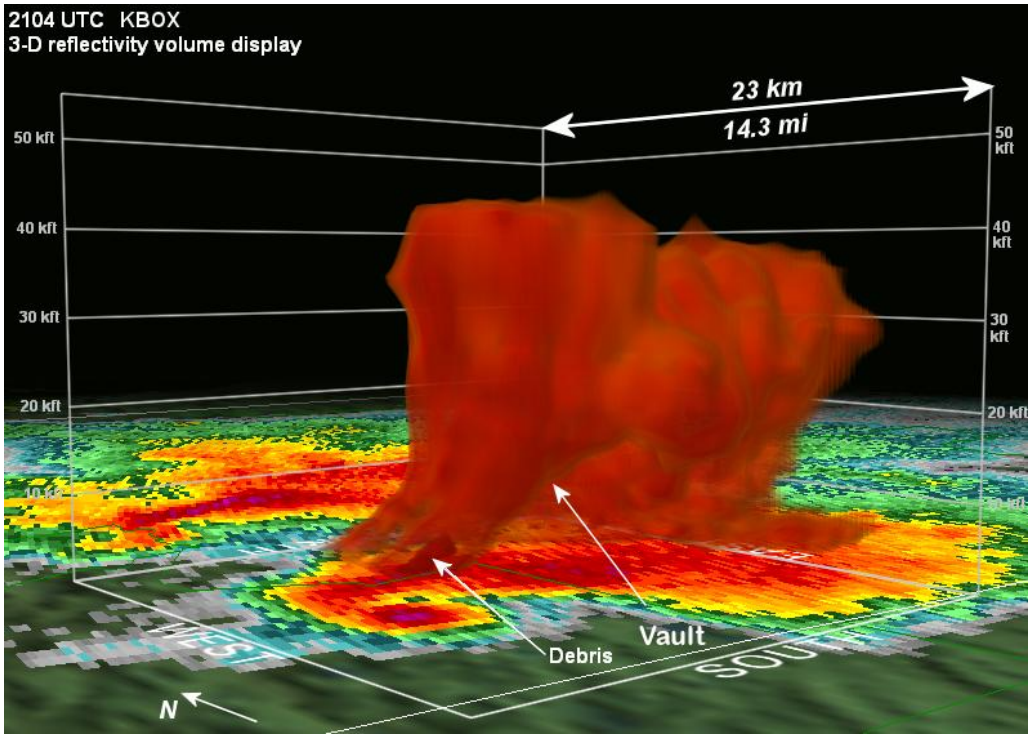

Figure 25: BOX reflectivity volume display at 2104 UTC showing radar evidence of lofted debris in the low levels of the mesocyclone. Reflectivity values >50 dBZ are shown. *Click image to enlarge.*

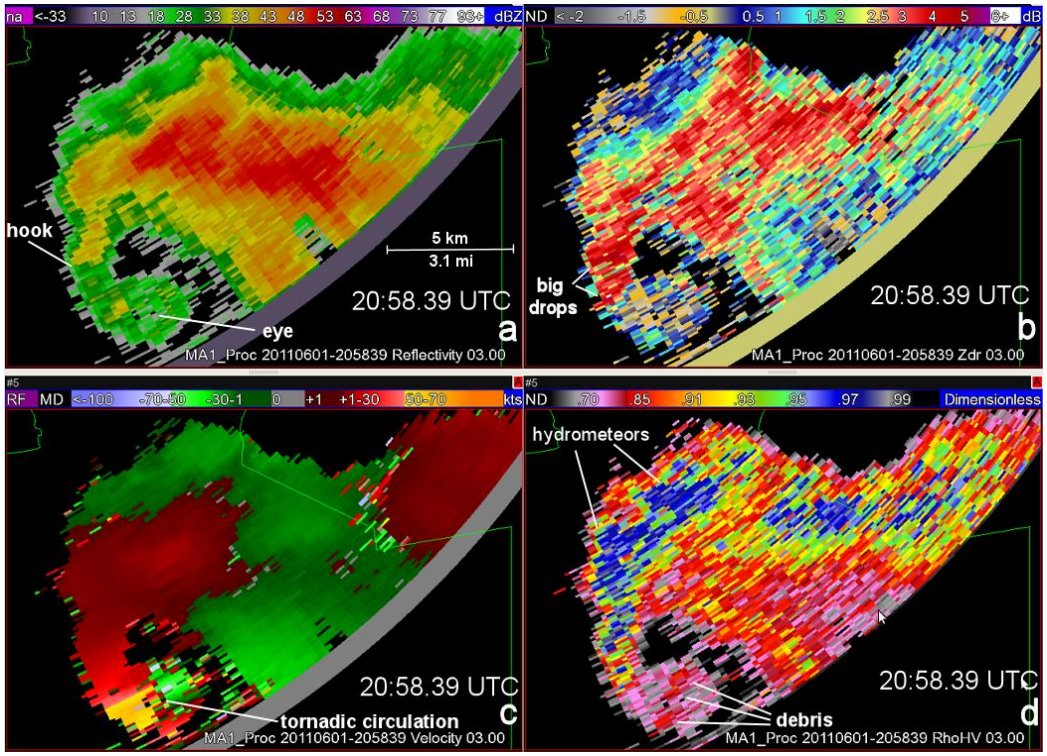

Figure 26: CASA MA1 at 2058 UTC 1 June 2011 showing a) reflectivity, b) differential reflectivity (Z_{DR}), c) velocity, and d) correlation coefficient (ρ_{hv}) of the strong tornado near Monson, MA. *Click image to enlarge.* QuickTime loops are available here: reflectivity, differential reflectivity (Z_{DR}), velocity, and correlation coefficient (ρ_{hv}).

The tornado became more destructive as it headed into West Springfield around 2032 UTC. Extensive damage occurred to industrial buildings and homes in the Union Street neighborhood near the rail yard. The roofs of several brick buildings were removed and multi-story buildings lost their upper levels. Many homes were pushed off their foundations and flattened, including one with a fatality. Damage in West Springfield was classified as EF2 with estimated wind speeds of 50–60 m s^{-1} (111 to 135 mph).

As the tornado continued to track eastward, it crossed the Memorial Avenue Bridge near the rotary around 2034 UTC. There was a considerable amount of traffic on the bridge during the afternoon rush hour. Eyewitnesses reported a tractor trailer blown over on the bridge. Other drivers attempted to reverse their cars upon seeing the tornado approach. Once past the bridge, the tornado crossed the Connecticut River and into downtown Springfield, an event captured by a local television station's webcam (see: www.wwlp.com/dpp/news/video-june-1-2011-tornado). Many homes and businesses were destroyed in the south side of the downtown area along Main Street, between Winthrop Street and Howard Street. Several commercial brick buildings in this area sustained major damage. The tornado produced severe structural damage to townhomes and apartments near Springfield College. Farther east, the Island Pond section of the city sustained the most significant damage. Some homes were either damaged by fallen trees or pushed off their foundations. Cathedral High School suffered severe damage to its roof and a section of a brick wall collapsed. Damage in Springfield was rated EF2 with estimated wind speeds of 50–60 m s^{-1} (111–135 mph).

Tornado damage strengthened eastward through Wilbraham and Monson between 2040–2100 UTC. In Wilbraham, the most severe damage occurred near the town line with Hampden, where there was deforestation and significant damage to nearby structures. One person died at a campground after seeking shelter in a trailer. The tornado continued directly through Monson (Fig. 2). Widespread damage occurred to commercial buildings and homes, some of which were destroyed (Fig. 27). Parts of the town experienced near-complete deforestation, with tree bark stripped from some remaining trunks. Damage in these towns was classified as EF3 with estimated wind speeds of 61–74 m s^{-1} (136–165 mph).

Substantial deforestation occurred in the Brimfield State Forest around 2105 UTC, where the tornado reached its maximum width of approximately 0.8 km (0.5 mi) with EF3 damage along Holland Road. Damage here was near the time and location of the best defined BOX 0.5° debris spike (2104 UTC, Fig. 22), and also was associated with ground scarring as seen in satellite imagery (Fig. 28). Damage to structures and forested areas continued for several miles in Brimfield (Fig. 29) and Sturbridge, where the tornado crossed Interstate 84. Trees and several tractor trailers were blown over, and a highway sign was twisted. Farther east, the tornado crossed Southbridge Airport, tossing small aircraft into the woods east of the airport. Damage in these areas was classified as EF2 with estimated wind speeds of 50–60 m s^{-1} (111–135 mph). The tornado dissipated in the southwest part of Charlton around 2127 UTC.

Figure 27: Tree and property damage in Monson, MA estimated at EF3. Tornado exited over the ridge and narrowed at right on photo. [Photo by Joe Dellicarpini.] *Click image to enlarge.*

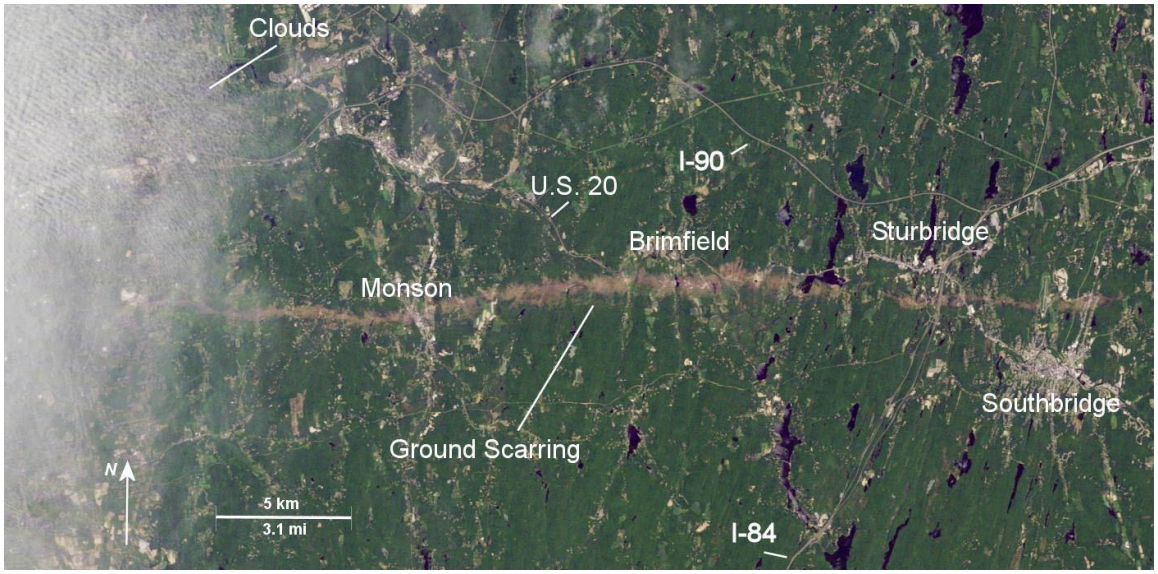

Figure 28: NASA Landsat 5 Thematic Mapper natural-color image taken on 8 June 2011 showing ground scarring up to 0.5 mi (0.8 km) wide from the long-tracked EF3 tornado on 1 June 2011 across south-central MA. The western portion of tornado damage track is obscured by clouds. *Click image to enlarge.*

6. Discussion and summary

The severe weather outbreak of 1 June 2011 was climatologically atypical, producing the 3rd highest DPI over eastern New York and New England since 1950, as well as a record number of significant hail reports (≥5.1 cm, ≥2 in) over the region. A favorable environment for supercells was established by a combination of steep mid-level lapse rates associated with an EML, steep low-level lapse rates with strong boundary-layer heating, rich boundary-layer moisture (surface dewpoints 20–22°C), and increasing vertical shear profiles associated with an approaching shortwave trough from the west. This event meets the EML-associated significant-severe weather criteria established by Banacos and Ekster (2010), and is consistent with their overall synoptic pattern. A terrain-induced prefrontal trough and strong normal component of deep-layer shear vectors (in the absence of strong linear forcing) favored supercells. Surface pressure falls and strengthening wind fields led to strong near-surface directional and speed shear east of the prefrontal trough and near the instability axis across New England, contributing to the occurrence of six tornadoes, including one EF3.

Convective parameters on 1 June 2011, including SRH, EHI, VGP, LCL height, and 0–1-km bulk shear, were consistent with ranges found in significant-tornado proximity sounding studies. Further, refined convective parameters (Rasmussen 2003) such as 0–1-km SRH and 0–3-km CAPE, and composite parameters such as STP (Thompson et al. 2003) and EHI, were also shown to be potentially useful. In terms of short-term forecasting value, these parameters correctly highlighted the areas of greatest concern for tornadoes.

Figure 29: Aerial view of significant damage to trees and homes in Brimfield, MA rated EF3. [Photo by Civil Air Patrol/David Manning.] *Click image to enlarge.*

While the debris spike was a unique feature, the conventional and dual-polarization radar signatures are otherwise consistent with tornadic storms observed elsewhere in similar environments. The dual-polarization products

along with higher spatial and temporal evolution details provided by the 3-cm wavelength CASA MA1 are worthy supplements to the WSR-88D data for analyzing low-level rotation and potential tornadoes, especially in terms of temporal detail (20-s scans).

Anticipation of rare events like 1 June 2011 is complicated by uncertainties concerning the mesoscale details (e.g., the convective mode, the observed rapid increase in 0–1-km AGL bulk shear, etc.). These details may not become apparent until the hours before event occurrence. However, some success in providing a generalized assessment of severe thunderstorm potential in New England is possible several days in advance, partly through tracking the plume of steep lapse rates associated with the EML in operational model forecasts[4]. Along those lines, the absence of standard trajectory analyses in NCEP post-processing—as existed in the past with the Nested Grid Model (Reap 1992)—appears to be a hindrance to easily determining low- and mid-level air mass origins and motion useful for a number of forecast applications. A resumption of standard trajectory analyses may be a worthy consideration for NWS operational workstations (i.e., Advanced Weather Interactive Processing System, AWIPS) and Internet dissemination to better monitor the potential collocation of favorable conditions (e.g., the trajectories bringing steep mid-level lapse rates and low-level moisture together as shown in Fig 7.).

There are several possible directions for future work stemming from this case study. First, a specific composite study of prefrontal troughs in northeastern U.S. severe weather events would be beneficial to clarify their potential contribution to the observed convective modes and low-level wind fields, as hypothesized in section 3a. Second, an operational model-based study of mid-tropospheric lapse rates, and their associated handling and/or biases, could aid short to medium range forecasts of severe weather in the northeastern U.S.. Third, some role of the terrain in channeling low-level flow and enhancing tornado potential has been presented with other significant tornadoes in the area (e.g., the Great Barrington tornado by Bosart et al., 2006). Reasoning for tornadoes related to orographic influences necessarily would be speculative here, given available observations, and would appear to be of secondary importance given the favorable mesoscale environment for significant tornadoes. In future work, the authors plan to examine the role of terrain-channeled flow on low-level mesocyclone strength using a high-resolution model.

[4]The SPC successfully highlighted the area starting with the Day 5 convective outlook, citing the EML as a component of the severe threat.

ACKNOWLEDGMENTS

The authors wish to thank Seth Binau, John Goff, Dave Radell, Paul Sisson, and Rick Watling for their helpful reviews and suggestions. A previous iteration of this paper reviewed by Richard Thompson and Kiel Ortega provided many helpful and detailed comments, which have led to the manuscript in its present form. Formal reviews provided by Lance Bosart, Matthew Kumjian, and Corey Mead were insightful and helped improve the paper. Editorial comments provided by Roger Edwards and David Schultz were also beneficial in clarifying some concepts. The NCEP-NCAR global reanalysis images were provided by the NOAA/ESRL Physical Sciences Division from their Web site (www.esrl.noaa.gov/psd/). The NOAA Air Resources Laboratory (ARL) READY website (www.arl.noaa.gov/ready.html) was used for the HYSPLIT trajectories.

Disclaimer. Reference to any specific commercial products, process, or service by trade name, trademark, manufacturer, or otherwise, does not constitute or imply its recommendation, or favoring by the United States Government or NOAA/National Weather Service. Information from this publication shall not be used for advertising or product endorsement purposes.

REFERENCES

U.S. Air Force, 1990: The use of the skew *t*, log *p* diagram in analysis and forecasting. AWS/TR79/006 (revised), Air Weather Service, 162 pp.

Banacos, P. C., and M. L. Ekster, 2010: The association of the elevated mixed layer with significant severe weather events in the northeastern United States. *Wea. Forecasting*, **25**, 1082–1102.

Blanchard, D. O., 1998: Assessing the vertical distribution of convective available potential energy. *Wea. Forecasting*, **13**, 870–877.

Bluestein, H. B, and M. L. Weisman, 2000: The interaction of numerically simulated supercells initiated along lines. *Mon. Wea. Rev.*, **128**, 3128–3149.

——, M. M. French, R. L. Tanamachi, S. Frasier, K. Hardwick, F. Junyent, A. L. Pazmany, 2007: Close-range observations of tornadoes in supercells made with a dual-polarization, X-band, mobile Doppler radar. *Mon. Wea. Rev.*, **135**, 1522–1543.

Bosart, L. F., A. Seimon, K. D. LaPenta, and M. J. Dickinson, 2006: Supercell tornadogenesis over complex terrain: The Great Barrington, Massachusetts, tornado on 29 May 1995. *Wea. Forecasting*, **21**, 897–922.

Bothwell, P. D., J. A. Hart, and R. L. Thompson, 2002: An integrated three-dimensional objective analysis scheme in use at the Storm Prediction Center. Preprints, *21st Conf. on Severe Local Storms*, San Antonio, TX, Amer. Meteor. Soc., J117–J120.

Bunkers, M. J., and M. A. Baxter, 2011: Radar tornadic debris signatures on 27 April 2011. *Electronic J. Operational Meteor.*, **12** (7), 1–6. [Available online at www.nwas.org/ej/pdf/2011-ION1.pdf]

Cannon, J. W., 2002: Characteristics of recent northern New England tornadoes. Eastern Region Tech. Attachment 2002-04, 16 pp. [Available online at www.erh.noaa.gov/er/hq/ssd/erps/ta/ta2002-04.pdf]

Carlson, T. N., and F. H. Ludlam, 1968: Conditions for the occurrence of severe local storms. *Tellus*, **20**, 203–226.

Craven, J. P., and H. E. Brooks, 2004: Baseline climatology of sounding derived parameters associated with deep, moist convection. *Nat. Wea. Digest*, **28**, 13–24.

Davies, J. M., 1993: Hourly helicity, instability, and EHI in forecasting supercell tornadoes. Preprints, *17th Conf. on Severe Local Storms*, St. Louis, MO, Amer. Meteor. Soc., 107–111.

Dial, G. L., J. P. Racy, and R. L. Thompson, 2010: Short-term convective mode evolution along synoptic boundaries. *Wea. Forecasting*, **25**, 1430–1446.

Doswell, C. A. III, and D. M. Schultz, 2006: On the use of indices and parameters in forecasting severe storms. *Electronic J. Severe Storms Meteor.*, **1** (3), 1–22.

——, R. Edwards, R. L. Thompson, J. A. Hart, and K. C. Crosbie, 2006: A simple and flexible method for ranking severe weather events. *Wea. Forecasting*, **21**, 939–951.

Dowell, D. C., C. R. Alexander, J. M. Wurman, and L. J. Wicker, 2005: Centrifuging of hydrometeors and debris in tornadoes: Radar-reflectivity patterns and wind-measurement errors. *Mon. Wea. Rev.*, **133**, 1501–1524.

Draxler, R. R., and G. D. Hess, 1997: Description of the HYSPLIT_4 modeling system. NOAA Tech. Memo. ERL ARL-224, 24 pp. [Available online at www.arl.noaa.gov/documents/reports/arl-224.pdf]

——, and ——, 1998: An overview of the HYSPLIT_4 modeling system for trajectories, dispersion, and deposition. *Aust. Meteor. Mag.*, **47**, 295–308.

Farrell, R. J., and T. N. Carlson, 1989: Evidence for the role of the lid and underrunning in an outbreak of tornadic thunderstorms. *Mon. Wea. Rev.*, **117**, 857–871.

Fujita, T. T., 1973: Proposed Mechanism of tornado formation from rotating thunderstorms. Preprints, *8th Conf. on Severe Local Storms,* Denver, CO, Amer. Meteor. Soc., 191–196.

Janjić, Z. I., 2003: A nonhydrostatic model based on a new approach. *Meteor. Atmos. Phys.*, **82,** 271–285.

Johns, R. H., and R. A. Dorr, 1996: Some meteorological aspects of strong and violent tornado episodes in New England and eastern New York. *Natl. Wea. Dig.*, **20** (4), 2–12.

Kalnay, E., and Coauthors, 1996: The NCEP/NCAR reanalysis 40-year project. *Bull. Amer. Meteor. Soc.*, **77**, 437 –471.

Kumjian, M. R., 2011: Precipitation properties of supercell hook echoes. *Electronic J. Severe Storms Meteor.*, **6** (5), 1–21.

Lanicci, J. M. and T. T. Warner, 1991a: A synoptic climatology of the elevated mixed layer inversion over the southern Great Plains in spring. Part 1: Structure, dynamics and seasonal evolution. *Wea. Forecasting*, **6**, 181–197.

——, and ——, 1991b: A synoptic climatology of the elevated mixed layer inversion over the southern Great Plains in spring. Part 2: The life cycle of the lid. *Wea. Forecasting*, **6**, 198–213.

——, and ——, 1991c: A synoptic climatology of the elevated mixed layer inversion over the southern Great Plains in spring. Part 3: Relationship to severe-storms climatology. *Wea. Forecasting*, **6**, 214–226.

Lemon, L. R., 1998: The radar "three-body scatter spike": An operational large-hail signature. *Wea. Forecasting*, **13**, 327–340.

——, and C. A. Doswell III, 1979: Severe thunderstorm evolution and mesocyclone structure as related to tornadogenesis. *Mon. Wea. Rev.*, **107**, 1184-1197.

Lewellen, D. C., B. Gong, and W. S. Lewellen, 2008: Effects of finescale debris on near-surface tornado dynamics. *J. Atmos. Sci.*, **65**, 3247–3262.

Locatelli, J. D., R. D. Schwartz, M. T. Stoelinga, P. V. Hobbs, 2002: Norwegian-type and cold front aloft–type cyclones east of the Rocky Mountains. *Wea. Forecasting*, **17**, 66–82.

Markowski, P. M., E. N. Rasmussen, J. M. Straka, and D. O. Blanchard, 1998: Variability of storm-relative helicity during VORTEX. *Mon. Wea. Rev.*, **126**, 2959–2971.

——, C. Hannon, J. Frame, E. Lancaster, A. Pietrycha, R. Edwards, and R. L. Thompson, 2003: Characteristics of vertical wind profiles near supercells obtained from the Rapid Update Cycle. *Wea. Forecasting*, **18**, 1262–1272.

McDonald, J. R., K. C. Mehta, and S. Mani, 2003: F-scale modification process and proposed revisions. Preprints, *Symp. on the F-Scale and Severe-Weather Damage Assessment*, Long Beach, CA, Amer. Meteor. Soc., 1.1.

McLaughlin, D., and Coauthors, 2009: Short-wavelength technology and the potential for distributed networks of small radar systems. *Bull. Amer. Meteor. Soc.*, **90**, 1797–1817.

Palmer, R. D., and coauthors, 2011: Observations of the 10 May 2010 tornado outbreak using OU-PRIME. *Bull. Amer. Meteor. Soc.*, **92**, 871–891.

Rasmussen, E. N., 2003: Refined supercell and tornado forecast parameters. *Wea. Forecasting*, **18**, 530–535.

——, and D. O. Blanchard, 1998: A baseline climatology of sounding-derived supercell and tornado forecast parameters. *Wea. Forecasting*, **13**, 1148–1164.

Reap, R. M., 1992: The Meteorological Development Laboratory three-dimensional trajectory model. NOAA Tech. Procedures Bull. 397, 11 pp. [Available from NWS Office of Climate, Water, and Weather Services, 1325 East-West Highway, Silver Spring, MD 20910]

Ryzhkov, A. V., T. J. Schuur, D. W. Burgess, and D. S. Zrnić, 2005: Polarimetric tornado detection. *J. Appl. Meteor.*, **44**, 557–570.

Schenkman, A. D., M. Xue, A. Shapiro, K. Brewster, and J. Gao, 2011: Impact of CASA radar and Oklahoma Mesonet data assimilation on the analysis and prediction of tornadic mesovortices in an MCS. *Mon. Wea. Rev.*, **139**, 3422–3445.

Schultz, D. M., 2005: A review of cold fronts with prefrontal troughs and wind shifts. *Mon.Wea. Rev.*, **133**, 2449–2472.

——, 2010: How to research and write effective case studies in meteorology. *Electronic J. Severe Storms Meteor.*, **5** (2), 1–18.

Smith, T. M., and K. L. Elmore, 2004: The use of radial velocity derivatives to diagnose rotation and divergence. Preprints, *11th Conf. on Aviation, Range, and Aerospace Meteorology*, Hyannis, MA, Amer. Meteor. Soc., P5.6.

Snellman, L. W., 1982: Impact of AFOS on operational forecasting. Preprints, *Ninth Conf. on Weather Forecasting and Analysis*, Seattle, WA, Amer. Meteor. Soc., 13–16.

Thompson, R. L. and M. D. Vescio, 1998: The destruction potential index - A method for comparing tornado days. Preprints, *19th Conf. on Severe Local Storms*, Minneapolis, MN, Amer. Meteor. Soc., 280–282.

——, R. Edwards, J. A. Hart, K. L. Elmore, and P. M. Markowski, 2003: Close proximity soundings within supercell environments obtained from the Rapid Update Cycle. *Wea. Forecasting*, **18**, 1243–1261.

Wang, Y., and V. Chandrasekar, 2010: Quantitative precipitation estimation in the CASA X-band dual-polarization radar network. *J. Atmos. Oceanic Technol.*, **27**, 1665–1676.

Wilson, J. W., and D. Reum, 1986: "The hail spike": Reflectivity and velocity signature. Preprints, *23rd Conf. on Radar Meteorology*, Snowmass, CO, Amer. Meteor. Soc., 62–65.

——, and ——, 1988: The flare echo: Reflectivity and velocity signature. *J. Atmos. Oceanic Technol.*, **5**, 197–205.

Zrnic, D. S., 1987: Three-body scattering produces precipitation signature of special diagnostic value. *Radio Sci.*, **22**, 76–86.

REVIEWER COMMENTS

[Authors' responses in *blue italics.*]

REVIEWER A (Matthew R. Kumjian):

Initial Review:

Recommendation: Accept with minor revisions.

Summary: The authors have substantially revised an earlier manuscript, and in my opinion the current version is more focused, better organized, and well written. The authors present a case study of the 1 June 2011 tornado outbreak in New England, following the "forecast funnel" approach by working from the synoptic scale down to the storm scale. The majority of my comments are minor and should be relatively easy to address.

Substantive comments:

The 2 y^{-1} statistic about significant tornadoes is quite surprising. A quick count from Table 1 reveals that more than half of the 142 tornadoes occurred on those 20 days listed. So, perhaps it may be beneficial to clarify the number of significant *tornado days*, or, the median number of significant tornadoes per year, as the average appears high owing to outbreak days. By the way, the context with outbreaks from other parts of the country definitely helps, so kudos.

A few points: First, please note that Table 1 lists the total number of tornadoes for each top-20 event day, not just F2 or greater tornadoes. Thus, it's not the case that more than half the F2 or greater tornadoes occurred among these top-20 event days. Also, there was a slight westward change in the domain (to capture a long-tracked tornado on 10 July 1989 that was not included previously since part of the tornado track was outside the domain) such that we now have a revised total of 150 F2 or greater tornadoes since 1950 (the text has been updated accordingly). We computed 108 individual significant-tornado event days (1.7 y^{-1}). The median was 1 y^{-1}. These values have been included in the revised manuscript. Interestingly, the database shows many more F2 or greater event days during the first half of the time period (1950–1980 had 85, 1981–2011 had just 23). Obviously, there are inconsistencies in the reporting of tornadoes and NWS verification methods over the span of six decades that would make it difficult to extract any meaningful climatological trend in these values.

Do you expect the tornadic debris signatures to differ based on geographical region? I would argue that differences in the precipitation characteristics of the storm stand a better chance of differing from one geographic region to another (though, admittedly, I am skeptical that they do in a significant way).

We've removed this statement. There might be differences in the debris signatures, but likely only to the extent that the nature of the vegetative cover being affected by the tornado differs. There was certainly something "different" about the reflective properties of the TDS near Brimfield, MA to cause the debris spike in the KBOX WSR-88D reflectivity data, though we've only been able to speculate about the reason for this unique observation. It's certainly not the first tornado to move through a state forest. In light of the uncertainties, we've chosen not to highlight this.

The textbook of Markowski and Richardson (2010) has a nice review of the lapse rate tendency equation and the physical meaning of terms, so it may be worth citing.

Thanks for the information. Banacos and Ekster (2010) also presents the lapse rate tendency equation and physical meaning. As an aside, the lead author believes he and Paul Markowski can probably both trace back our discussion of this equation to a homework assignment in Chuck Doswell's advanced forecasting techniques class we took at OU in 1997. The original published reference of the equation (i.e., the one deserving most credit) that we are aware of is the Air Weather Service technical document from 1990, which gives quite a detailed description. We've opted to stick to the original paper here.

This may be a misunderstanding on my part, but I don't understand what is meant by "longitudinal cloud bands" from Fig. 10. They appear to be oriented from SW to NE…

We've retained the original descriptor here. A longitudinal cloud band is one that is oriented parallel to the boundary layer shear vector (e.g., cloud streets); whereas transverse cloud bands align perpendicular to the shear vectors (e.g., horizontal convective rolls or bands sometimes seen in cirrus clouds near the upper-tropospheric jet).

I do not know what "deeper cloud-bearing shear" is referring to. Shear in the cloud-bearing layer? Please clarify.

Shear in the cloud-bearing layer was the intended wording and it has been fixed.

Figure 10 caption: What do you mean by "buoyancy waves"? They are not mentioned in the text, and I don't see anything in the satellite image. Please describe/explain in the text or remove from the figure caption.

Buoyancy waves are evident as transverse cloud bands, and occur due to oscillations in the weak capping inversion layer present at the time of the visible satellite image (1545 UTC). The wave clouds [were] subtle (but visible) in the Connecticut River valley of Massachusetts and across central Pennsylvania. This has been discussed in the revised text.

Discussion on parameters: There are some that may take issue with the use of these parameters (e.g., Doswell and Schultz 2006, EJSSM). Though I understand the desire to be thorough here, a lot of the parameters are using some of the same "ingredients", making them (in some cases) a bit redundant. I'm not suggesting an action item here; it's just more of an "awareness" sort of comment.

[Editor's note: The reviewer has a valid point here—one that probably could be addressed with a brief statement justifying the use of both the more basic ingredients and the derived indices, in light of the Doswell and Schultz (2006) precautions.]

Good points. We've added a disclaimer to open Section 3b and reference Doswell and Schultz (2006) for further elaboration on the potential issues. Please note that there is value in assessing convective parameters in areas of low climatological significant tornado frequency to see how they perform, since some geographic areas make up only a very small percentage of the sample used to generate the percentile rank analyses presented in the referenced proximity studies. Also note that Doswell and Schultz (2006) don't advocate abandoning the use of parameters and indices, but rightly point out that there is a lack of rigorous testing of diagnostic variables as forecast parameters in many instances that make their use problematic. Lastly, that there is a degree of "diagnostic overlap" in some of the parameters in not necessarily a deficiency. An ensemble approach should give a more confident diagnosis of the environment as simplifications associated with any one index (or data source) may lead a forecaster astray in a real-time situation.

The discussion here about topographic effects may not be necessary, as you say it is speculative given a (lack) of available data. In addition, given that this kind of environment in regions where topography probably doesn't play a role (e.g., the Great Plains) almost surely would produce tornadic supercells, I'm not sure there's even a strong case for any role of topography. I'd recommend removing this portion of the text, because I don't think it adds to the discussion.

This comment about topographic effects is at odds with that of another reviewer. We've retained mention to make clear we've considered terrain effects but simply don't have the available data to make any conclusive statements. Based on the prevailing environment, we don't believe terrain induced flow played a very large role for this event. Terrain induced flow and tornadogenesis is an area ripe for future investigation. The authors are planning to pursue this further in a separate study using a high resolution model.

Table 2: As a nice summary of the associated text, I suggest including the approximate percentiles (based on parameter studies) within which these observed values fall.

We've opted not to include this since the percentile rankings would come from different proximity studies depending on the parameter. This makes the information difficult to organize in tabular form. We feel the discussion is best left in the text.

Description of "debris ball": Ryzhkov et al. (2005; JAM) do not use the term "debris ball." At the recent AMS conference, Greg Forbes had a poster about the "debris ball" that may be online. Also, it might be too strong to say it is "*usually* an indicator that a *large* tornado is occurring".

Editor's note: the most commonly accepted term, and more literally accurate one, has become "tornadic debris signature", both in operations (http://wdtb.noaa.gov/courses/dualpol/Applications/TDS/player.html) and in literature, e.g.:

Bunkers, M. J., and M. A. Baxter, 2011: Radar tornadic debris signatures on 27 April 2011. *Electronic J. Operational Meteor*., **12** (7), 1–6.

We've made some wording change to clarify the TDS section. It wasn't our intention to imply the term "debris ball" appeared in Ryzhkov et al. (2005), but wanted to parenthetically include the colloquial usage. With the revisions, this should no longer be implied.

I found it momentarily confusing that the debris spike had outbound velocities in Fig. 18 but inbounds in Fig. 20, until I noticed that the former displayed storm-relative velocities and the latter is a display of base velocity. You may want to emphasize that difference.

The layout of the radar products is how we would like them presented. We've rechecked the annotations for what are now the captions for Figs. 22 and 24 and feel they are adequate, though we apologize for the initial confusion expressed by the reviewer.

3–4 dB values of Z_{DR} indicate probably more "medium to large" sized drops than "small". Note that Z_{DR} in rain at X band is actually quite similar to at S band. Also, >5 dB probably indicates some small melting hail mixed in as well.

We agree. The Z_{DR} interpretation discussion has been modified.

The first paper to document the tornadic debris in polarimetric data is Ryzhkov et al. (2005; JAM). Though I appreciate the reference, the Kumjian (2011, EJSSM) paper probably isn't the best reference here. You could move it down to the bottom of the page, as that paper discusses the strong heterogeneities in precipitation characteristics in hook echoes. Better references for the polarimetric debris signature include Bluestein et al. (2007, MWR—particularly relevant as it presents observations at X band), and Kumjian and Ryzhkov (2008, JAMC).

Bluestein et al. (2007) reference added for excellent X-band correlation coefficient observations and Kumjian (2011) cited with respect to ongoing research pertaining to processes affecting the precipitation distribution within hook echoes, which is now observable with dual-polarization.

[Minor comments omitted...]

Second review:

Recommendation: Accept with minor revisions.

Substantive comment: There is still a bit of confusion with the verbiage for the TDS and debris ball, and I'm afraid I may have contributed to it. It can be corrected by replacing "TDS" with "debris ball". The TDS has been used to describe the polarimetric debris signature, which is an unambiguous indicator of a damaging tornado. The "debris ball" often indicates a tornado, but is not unambiguous, as described in Bunkers and Baxter 2011.

We've changed the debris ball discussion consistent with the reviewer's thoughts, restricting the more precise tornadic debris signature (TDS) wording to describe the availability of correlation coefficient data

from dual-pol radar. While the TDS terminology has been used somewhat loosely in the past (i.e., without *the benefit of dual-pol data), it seems likely that the nomenclature will evolve in the manner described by the reviewer as dual-pol radars become operational across the United States.*

[Minor comment omitted…]

REVIEWER B (Corey M. Mead)

Recommendation: Accept with major revisions.

Substantive comments:

According to Schultz (2010), this manuscript has many characteristics of a good case study. However, deficiencies exist. After major revision, I would recommend publication.

As stated in the introduction, this paper supplements Banacos and Ekster (2010) with a multi-scalar case study which provides examples of observations from emerging radar products and platforms. However, based on the title of the paper, it is unclear to me whether the primary subject of investigation is the tornado or the entire severe weather episode? In either case, I find it hard to justify the disproportionate amount of discussion about the EML in Section 2, "Synoptic Setting and EML Advection." There is no question that the presence of an EML can be an important characteristic of a significant severe weather environment. But, I do feel that the evolution of the vertical wind profile, and boundary layer moisture profile (which you briefly addressed through backwards trajectory analysis) deserve equal discussion.

To support this notion, please consider the attached figures that were generated from archived SPC mesoanalysis data (see Dean et al. 2006, Schneider and Dean 2008, and Schneider et al. 2006). Fig. 1 is a plot of EF2+ tornado reports from 1 January 2003—31 December 2011 associated with 700–500-hPa lapse rates of <6.9 ºC km^{-1}. Fig. 2 is the same as Fig. 1, except for 700–500-hPa lapse rates >7.5ºC km^{-1}. For the 9-y period, there were nearly three times more EF2+ tornadoes that occurred in the weaker midlevel lapse rate environment. And despite the much less prominent discussion about the low-level shear and moisture (relative to the EML), Fig. 3 shows that the cited values of MLLCL and 0–1 km bulk shear in Section 3 have a much better correlation to EF2+ tornado occurrence than the steep midlevel lapse rates (Fig. 2).

In summary, this is a nice case study that supplements the Banacos and Eskter (2010) work. It can be argued that the magnitude of this severe weather event should not be surprising, given the documented mesoscale environment. But, this case meets the three criteria put forth by National Weather Service Science and Operations Officer Jon Zeitler (as cited in Schultz 2010): (i) a unique or rare occurrence of a weather event., (ii) a demonstration of how new or unusual observations can be used to identify, analyze, or forecast an event (e.g., the dual-pol and CASA radar observations), and (iii) a demonstration of how theory can be applied, especially for unusual cases (e.g., the evolution and advection of the EML).

However, I feel that the authors are trying too hard to push the importance of the EML on the reader at the expense of a better discussion on the evolution of the vertical wind profile and low-level moisture profile, which are arguably better correlated to significant tornado occurrence. This is especially the case in Section 2, which documents the synoptic-scale pattern evolution, where I would like to see a more balanced, ingredients-based approach.

References:

Banacos, P. C., and M. L. Ekster, 2010: The association of the elevated mixed layer with significant severe weather events in the Northeastern United States. *Wea. Forecasting*, **25**, 1082-1102.

Dean, A.R., R.S. Schneider, and J.T. Schaefer*, 2006: Development of a Comprehensive Severe Weather Forecast Verification System at the Storm Prediction Center. *Preprints*, 23nd Conf. Severe Local Storms, St. Louis MO.

Schneider, R.S., and A.R. Dean, 2008: A Comprehensive 5-year Severe Storm Environment Climatology for the Continental United States. *Preprints*, 24th Conf. Severe Local Storms, Savannah GA.

Schneider, R.S., A.R. Dean, S.J. Weiss, and P.D. Bothwell, 2006: Analysis of Estimated Environments for 2004 and 2005 Severe Convective Storm Reports. *Preprints*, 23rd Conf. Severe Local Storms, St. Louis MO.

Schultz, D. M., 2010: How to research and write effective case studies in meteorology. *Electronic J. Severe Storms Meteor.*, **5** (2), 1–18.

The authors thank Corey for his thorough and insightful review. We've made a number of changes in response to the substantive comments provided. Here is an overview of those changes:

1.) The title has been revised to better indicate that the paper is an analysis of the entire severe weather event, while also suggesting to the reader that the long-tracked EF3 tornado would be a centerpiece of the paper. The title is somewhat more generic now, but should better convey the scope of the paper to the reader.

2.) The reviewer is concerned that there isn't sufficient focus on the low-level shear and boundary layer moisture profile in the near-storm environment. We believe the EML is an important feature for forecasters to be aware of, but we agree with the reviewer that the low-level shear, LCL heights, and convective mode have a better (and more direct) association with significant tornado occurrence than does the EML.

We've worked on further balancing the discussion. Specifically, we've included time series discussion of the OKX and BOX VAD winds (with data provided by the reviewer, see Fig. 13) to further highlight the important increase in low-level bulk shear during the afternoon hours on 1 June 2011. We've also included meteograms for ALB and BDL showing basic weather elements and hourly trends in 0-1km SRH and LCL height derived from ACARS data (and 12 and 16 UTC soundings from ALB, Figs. 12 and 16). We've removed explicit mention of "EML advection" from the title of section 2 to not imply greater importance of this feature. We would argue that it takes a bit more burden of evidence to document EML transport than it does low-level moisture transport, since the EML requires establishing a specific source mechanism. Thus, there is still a slant toward the EML in the discussion and state in the opening section that this case study is meant to compliment the EML composite study of Banacos and Ekster (2010). While not completely balanced, we've attempted to place further emphasis on the moisture and 0–1km bulk shear in the abstract, Sections 2–3, and in the concluding discussion, and to make it clear that these factors were of more direct consequence to the EF3 tornado. As an aside, we've been careful in this paper and in the Banacos and Ekster (2010) paper to keep the importance of the EML rooted in parcel theory, while not tying it to any specific convective mode. We've established previously that the presence of an EML makes significant severe weather more likely in the northeast U.S., but it's not a necessary condition. Some of the top-20 tornado events (Table 1) were associated with EMLs, others (e.g., 24 July 2008, 3 October 1979) were not. Here is something to consider though: four of the top five events in Table 1 were associated with an EML. Also, nearly 70% of the DPI in Table 1 occurred with documented EML events from 1970–present and the 9 June 1953 Worcester tornado case (we have not investigated the remaining events in the 1950s and 1960s).

3.) We've hopefully avoided suggesting "EML = tornado" implications. The EML does create a more "Plains-like" convective environment with the steeper mid-level lapse rates, and that is actually reflected in the distribution of tornadoes versus mid-level lapse rate provided in the reviewer's Figs. 2 and 3. It is clear that there are a variety of vertical temperature and moisture distributions associated with tornadoes (different parameter "subspaces"). We agree that measures such as the LCL height, 0–1km bulk shear, and the observed convective mode have a better relationship with the EF2+ tornado occurrence, and there is a more focused parameter space in association with those variables and tornadoes than there is with respect to mid-level lapse rate. Likewise, the presence of an EML says nothing about what convective mode to expect, which impacts favored severe weather types. The revisions place further emphasis on providing a diagnostic picture of low-level shear and thermodynamic conditions, especially with respect to the EF3 tornado.

4.) We've concluded Section 2 by stating that the large-scale pattern has brought together steep mid-level lapse rates and rich boundary layer moisture, yielding a strongly unstable environment. From the standpoint of discussing ingredients (moisture, instability, lift, and low-level shear), we feel these topics are all sufficiently covered in the revision.

Substantive specific comments:

This paper submitted that northeast U.S. tornadic outbreaks the magnitude of 31 May 1985 are modulated by the presence of the "lid" or EML. To assert that marginal CAPE is largely responsible for fewer tornadic supercells in the northeast U.S. seems somewhat speculative. What about all of the cool season tornado events in the southeast U.S.? Many of these cases are associated with poor midlevel lapse rates and weak CAPE.

We've reworded this slightly to say that factors mitigating CAPE are partly to blame for the lower climatological frequency of tornadic supercells in the northeast. We feel this is a fair statement. Mitigating factors include not only the lack of steep mid-level lapse rates but also the cool marine modified air masses that often affect New England on southeast flow. This is unlike the southeast U.S. in the cool season, where marine modified low-level air from the Gulf of Mexico can contribute in a positive sense toward CAPE (advection of higher theta-e from oceanic areas, even during the nighttime hours). We've documented a number of significant tornado events in the northeast associated with EMLs, and since EMLs generally lead to greater CAPE we feel the association is valid.

[Re: "Associated mid-level dry air can enhance evaporative cooling through entrainment, aiding in the intensity of convective downdrafts."] Numerical simulation results from James and Markowski (2010) dispute this claim. See http://journals.ametsoc.org/doi/pdf/10.1175/2009MWR3018.1.]

We thank the reviewer for mentioning this important work. We've read the paper and in keeping with the result, we've removed the mention of mid-level dry air enhancing evaporative cooling.

I like the idea of the backward trajectories for low-level air parcels. However, is there any way to qualify the claim of "rich low-level moisture?" Perhaps, through the use of a few observed soundings along the 1000-m trajectory; similar to Fig. 8.

We've quantified surface dewpoints throughout the paper. The surface dewpoints along the southeast Virginia and North Carolina coasts were near 21ºC the start of the low-level trajectories (30/12 UTC) shown in Fig.7. We have a lot of figures in the paper already, so we've avoided adding one here.

It might be instructive to incorporate 1200 UTC BUF and ALB soundings to describe the character of the ambient environment for the initiating, daytime storms. Modifying these soundings for surface conditions as of 1500 UTC suggests little or no remaining convective inhibition.

The discussion of the daytime convective initiation has been considerably revised. The CINH at 1200 UTC was significantly lower at BUF than ALB, and by 1500 UTC the environment across central New York was essentially uncapped. We've included this in the revised discussion.

[Re: "Many recent tornadic storms in New England have been documented along and downwind of pre-frontal troughs..."] What is the physical reasoning for this?

Another reviewer brought this up as well. We note this was an empirical finding. However, it's likely that there is greater directional shear east of the pre-frontal trough in most situations (differences in 0–1km SRH at BDL and ALB are consistent with this). There was also richer low-level moisture east of the pre-frontal trough, at least in this case. We've modified the discussion in Section 3a to include this. We note in the conclusions that a specific composite study of pre-frontal troughs associated with northeastern U.S. severe weather outbreaks would be a potential avenue of future work.

This [surface pressure falls contributing to strengthened low-level shear] is potentially an important point, and I would like to see evidence in observational data. If you wish, you can use either Fig. 4 or Fig. 5 from the attached comments. At KOKX, 0–1 km bulk wind difference increased from 9 m s^{-1} at 1600 UTC to

12 m s^{-1} at 1900 UTC to 15 m s^{-1} at 2100 UTC. At KBOX, 0–1 km bulk wind difference increased from 17 m s^{-1} at 1600 UTC to 19 m s^{-1} at 1900 UTC before diminishing to 16 m s^{-1} at 2100 UTC. At the least, please reference Fig. 12 to qualify this statement.

We've added Fig. 13 which quantifies the increase in the low-level shear profile during the afternoon hours. We thank the reviewer for providing these data. This also dovetails with the RUC-based SPC mesoanalysis 3-h change in surface–1-km bulk shear displayed in Fig. 15.

What process was contributing to the intensification of the low-level shear? [Y]ou mentioned that strong boundary layer heating led to further strengthening of the pre-frontal trough with pressure falls of 2–3 mb h^{-1} observed. Was this the primary mechanism?

We've elaborated by saying that "The increase in low-level shear was likely a result of the surface pressure falls and strengthening gradient between the weakening 700-hPa ridge and approaching trough from the Great Lakes".

[Minor comments omitted...]

Second review:

Recommendation: Accept.

General comments: The authors have satisfactorily addressed all of my previous concerns. As such, I recommend publication of the manuscript.

REVIEWER C (Lance F. Bosart):

Initial Review:

Reviewer recommendation: Publish after minor revision (and a few "medium-lite" revisions)

Synopsis: The authors have produced a very good paper that addresses the salient features of the 1 June 2011 significant tornado outbreak in New England that included the devastating Springfield, MA, tornado. For the most part, evidence-based arguments are used to support inferences and the findings and conclusions are supported by observations to the extent possible. The 88D and CASA radar analysis discussion in sections 4a,b is first rate as is the discussion of the damage track analysis in section 6. I learned something from reading this paper, something I can't say about a lot of papers that I get asked to review. Finally, my comments below are sorted into substantive issues that need to be addressed before publication and number of little things that can be resolved offline.

We thank Lance for his thought-provoking comments and suggestions. The review definitely helped improve the paper. Our point-by-point responses follow.

Substantive Issues:

1. An important conclusion of this paper is the finding that the surface flow east of the prefrontal trough (PFT) has a larger component of the surface flow normal to the 700-hPa flow than the surface flow between the PFT and the cold front. We infer from this surface and 700-hPa flow relationship that the directional shear must be stronger east of the PFT than west of the PFT from which we surmise then further surmise that the environment is more favorable for supercell organization and intensification once the individual storms reach and cross the PFT and are able to ingest warm, moist low-level air that is characterized by strongly turning clockwise hodographs in the sub cloud layer. It would be nice to know how many of the other 20 storms listed in Table 1 share this flow structure for perspective purposes and to help address representativeness issues.

This is a good point. We've made explicit mention of the more favorable directional shear that exists east of the pre-frontal trough (on p. 9 and p. 11). We agree a composite study would be interesting with regard

to pre-frontal troughs and severe weather in the northeast, in part to generalize these aspects of the wind field. To examine all 20 events listed in Table 1 would go beyond the scope of this study, but we've added the reviewer's idea to a list of ideas for future work in the conclusion (perhaps as a CSTAR project?).

2. The thermal structure of the PFT discussed in the opening paragraph of section 2 needs to be documented to establish how the thermal, pressure, and wind structure changed across the PFT as is passed from the Hudson Valley to the Connecticut Valley. A comparison of observations from stations west of the Berkshires (e.g., GFL, ALB, POU, DDH, AQW, RUT, and PSF) with stations east of the Berkshires (e.g., BDL, BAF, CEF, EEN, and ORE) to address this issue would likely be helpful. Detailed surface analyses between 1600–2000 UTC, along with selective meteograms, would likely be helpful in this endeavor.

We agree. We've added meteograms for ALB and BDL (Fig. 12), to highlight the higher dewpoints and consistent wind directions 170–180º east of the pre-frontal trough at BDL, which should be somewhat representative of the storm's inflow. At ALB, the pre-frontal trough passage occurs with a wind shift from 190–280º, along with rising temperatures and lowering dewpoints at 01/2000 UTC. This appears consistent with adiabatic warming playing a role in the existence of this pre-frontal trough, and supports it being largely a terrain induced feature.

To dovetail with this, we've also derived a time series of 0–1km SRH and LCL height for ALB and BDL (in Fig. 16). These airport stations afforded us numerous ACARS soundings, and two rawinsonde observations at ALB (at 1200 and 1600 UTC) to determine these parameters. These time series show a more favorable regime for significant tornado occurrence east of the pre-frontal trough, and findings have be elaborated on in Section 3b. We feel the two meteograms sufficiently highlight the key environmental differences near and ahead of the pre-frontal trough. We can appreciate the reviewer's request to see more surface analyses. We've attempted to maximize the electronic format of the journal by providing numerous loops containing hourly surface observations (e.g., Fig. 9, 10, 14f). We are a bit long on figures with 28 and hope the loops of the raw observational data with radar and satellite overlays will suffice.

3. Use of the 2.5º NCEP/NCAR reanalysis to compute the lapse rates shown in Fig. 6 is probably OK for a synoptic-scale analysis. At issue is whether the use of the NARR, RUC/HRRR, or the CFSR would permit more important lapse rate detail to be resolves, especially in the vicinity of important terrain features.

We checked, and the NARR data is yet to be made available by ESRL for 2011. Higher resolution than that afforded by the Global Reanalysis would be nice, but our premise is that the EML is a feature that can generally be tracked in synoptic-scale analyses. We aren't sure that there would be any important mesoscale details in the EML plume with respect to the terrain in the northeast, since the EML resides above the height of the local terrain (EML base near 725 hPa in PIT and ALB sounding data).

4. Your trajectory analysis [suggests that] it would be nice to establish the sensitivity of the trajectory analysis to the resolution of the gridded datasets used to compute the trajectories. For example, the trajectories ending at 200 and 500 m over BAF show evidence of terrain-channeled flow up the Connecticut River Valley, whereas as the trajectory ending at 1000 m over BAF does not and is more representative of the larger-scale flow in the upper part of the planetary boundary layer. More on this point later.

This is a fair point, but the sensitivity would be difficult to quantify. For the purposes of a case study, the observed soundings and RUC-based SPC mesoanalyses used to track the EML indicate that the trajectories are consistent with these other data sources. Subjectively, we've seen some sensitivity in the HYSPLIT model with respect to the gridded dataset used. The greater differences tend to occur when selecting between the available vertical motion fields in HYSPLIT (i.e., between isentropic, isobaric, or the model's vertical velocity data). Over time, we've generally preferred the HYSPLIT results using the model's vertical velocity data but readily admit this is our subjective view of the output.

5. The discussion in the first part of section 3a would be stronger if you could establish good evidence that synoptic-scale (QG) ascent was present to the west over central and western PA/NY in the vicinity of 1200 UTC 1 June. This conclusion is made on the bottom of p. 8 but no supporting evidence is provided.

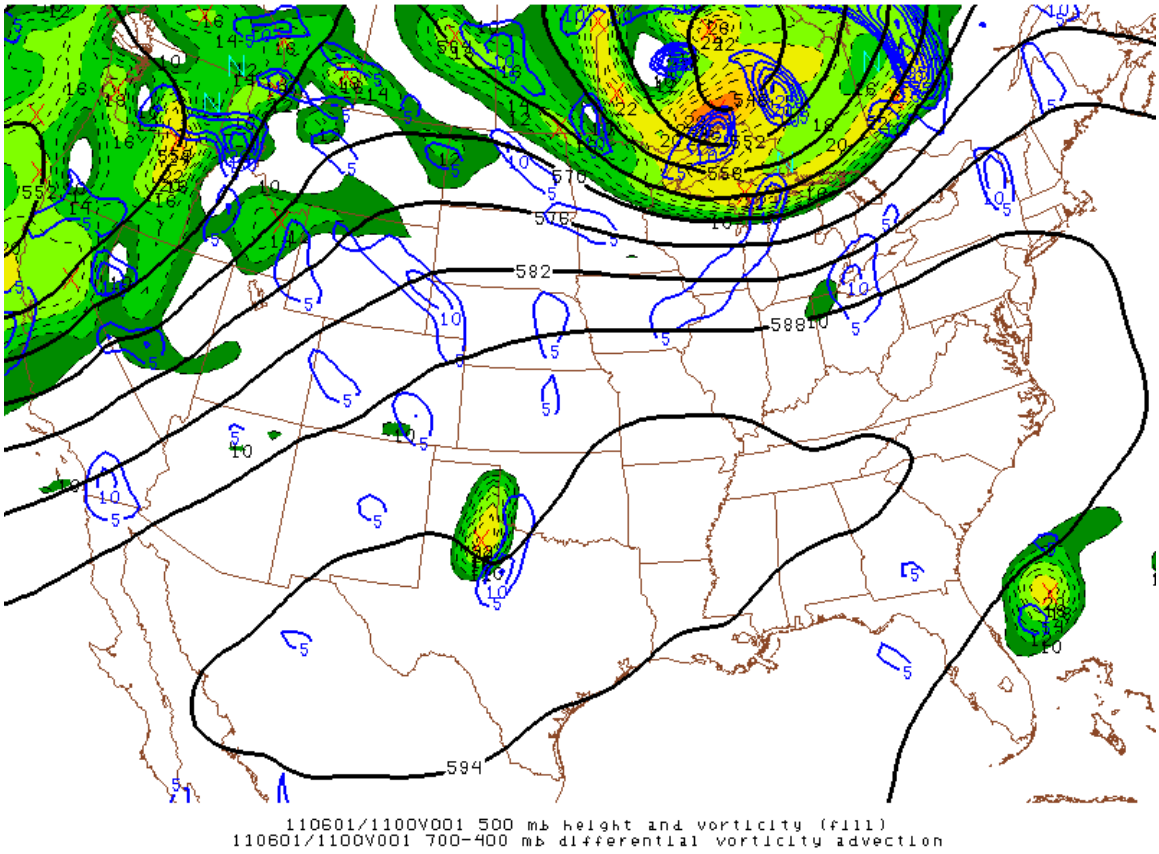

Above: RUC-based SPC mesoanalysis valid at 01/11 UTC.

From the RUC-based SPC mesoanalysis, there was an area of 700–400-hPa differential vorticity advection over northern New York that would suggest quasigeostrophic ascent. This feature had continuity, and is shown below at 11 UTC. There are also 700-500mb layer height falls during the 6-h period from 0600–1200 UTC over northern New York (about 40–50m/6-h). We've opted not to include this image in the paper since the early morning storms are a bit peripheral to the rest of the discussion.

6. Although you may very well be correct, I wouldn't be so quick to say that terrain-channeled flow appears unnecessary for the Springfield tornado case as you state. In our 2006 paper in WAF on the 1995 F3 Great Barrington, MA, tornado we make the point that the large-scale environmental flow has to be favorable for supercell development by itself in order to allow for the possibility that terrain-channeled southerly flow in the north-south oriented river valleys of eastern New York and western New England could act as a potential modifier of where a supercell might form or intensify. Lou Wicker has an important unpublished conference preprint from the late 1990s in which he showed with a preliminary modeling study that large directional shear in the 0–1 km layer could be associated with significant tornadoes (Lou: If you happen to read this review will you please go back and complete your modeling investigation and publish the results?). As possible evidence that terrain-channeled southerly flow may have been present in the Connecticut River Valley immediately prior to tornado genesis I have attached meter observations from BDL, BAF, CEF, and BDL for selected UTC times on 1 June. Although the surface winds are generally southerly ahead of the PFT at BAF and BDL, at both of these stations the winds appear to back by 10–20º ahead of the primary convective action. Similar behavior is suggested at CEF although the picture at this station is complicated by convectively contaminated surface winds. That said, it would be useful to determine whether the weakly backed surface winds at BAF and BDL ahead of the convection represent terrain-channeled flow and/or a dynamic response to the approaching convection. The only way to really address this issue properly in the absence of a dense mesoscale data network would be through a high-resolution simulation. I would add the special 1600 UTC 1 June ALB sounding shown in Fig. 14 strongly suggests the presence of terrain-channeled low level southerly flow up the Hudson River Valley. This

inference is even more evident when you go to the raw data and take a more careful look at the detailed wind profile from the surface to 850 hPa. Then there is Fig. 13. Almost all of the NSSL-indicated rotation tracks originate just east of the Hudson River Valley. Coincidence or enemy action?

The influence of terrain effects on tornadogenesis appears to be a continued research question. The extent to which a supercell thunderstorm is affected by terrain-channeled flow would likely depend on a number of factors, including the width/orientation of the valley, the prevailing environmental wind profile, surface roughness, and stability factors that would likely influence the dynamic response of the wind field to an approaching supercell and/or the response of the storm to any type of channeled inflow. Motivated by the varying comments in the reviews, we are in the process of pursuing a high resolution modeling approach to this rather than a more speculative discussion of any role of the terrain based on the available observational data we have for this case study. A modeling study would enable us to determine how a low-level mesocyclone might respond to systematic variations of the underlying terrain. A combination of a model simulation for a specific case and idealized simulations would be a worthy approach to the issue in our opinion. We'd like to talk to the reviewer about this further offline to incorporate possible ideas into the design of the next project.

Based on the reviewer's suggestions, we've rearranged this very brief discussion, placing the possible influence of terrain in the future work section. At this point, we come back to the fact that the mesoscale environment was broadly favorable for tornadoes. While we can't rule out the possible role of terrain-channeled flow in the initial tornadogenesis, the tornado strengthened as it moved out of the Connecticut Valley and into the hilly terrain to the east where presumably those effects would be less. As for the mesocyclone tracks beginning just east of the Hudson Valley, we believe this had to do with the greater concentration of storms east of the pre-frontal trough and the more favorable low-level directional shear.

7. Last but not least. I believe this paper would benefit from a more comprehensive mesoscale analyses that would include a detailed meteogram analysis for targeted stations. I would also suggest that a careful analysis of the HRRR 3-km analyses at forecast hours 3–6 (after the model has adjusted to the 0-h 12-km initialization) would likely prove to be enlightening.
[Listing of METAR observations omitted…]

We agree, and much of this is discussed in response to point #3. The addition of the meteograms (basic variables and derived parameters), VAD winds, and analyses of the dewpoint gradient along which storms initiated over central New York were all part of enhancing the mesoscale analyses included in the paper. An analysis of the accuracy of the various mesoscale models (including the HRRR) for this event would be interesting, but we feel that would be a separate study. We've attempted to keep our analysis observationally based to the extent possible.

[Minor comments omitted...]

Second review:

Recommendation: Accept with minor revisions.

[Minor comments omitted…]